Methods and Applications of Nanoelectrochemical Techniques

by

Christopher Madden

A Dissertation Presented in Partial Fulfillment
of the Requirements for the Degree
Doctor of Philosophy

Approved April 2012 by the
Graduate Supervisory Committee:

Thomas Moore, Chair
Anne Jones
Nongjian Tao

ARIZONA STATE UNIVERSITY

May 2012

ABSTRACT

Hydrogenases catalyze the interconversion of protons, electrons, and hydrogen according to the reaction: $2H^+ + 2e^- \leftrightarrows H_2$ while using only earth abundant metals, namely nickel and iron for catalysis. The enzymatic turnover of *Clostridium acetobutylicum* [FeFe]-hydrogenase has been investigated through the use of electrochemical and scanning probe techniques. Scanning tunneling microscopy (STM) imaging revealed sub-monolayer surface coverage. Cyclic voltammetry yielded a catalytic, cathodic hydrogen production signal similar to that observed for a platinum electrode. From the direct observation of single enzymes and the macroscopic electrochemical measurements obtained from the same electrode, the apparent turnover frequency (TOF) per single enzyme molecule as a function of potential was determined. The TOF at -0.7 V vs. Ag/AgCl for the four SAMs yielded a decay constant for electronic coupling (β) through the SAM of ~ 0.82 $Å^{-1}$, in excellent agreement with published values for similar SAMs.

One mechanism used by plants to protect against damage is called nonphotochemical quenching (NPQ). Triggered by low pH in the thylakoid lumen, NPQ leads to conversion of excess excitation energy in the antenna system to heat before it can initiate production of harmful chemical species by photosynthetic reaction centers. Here a synthetic hexad molecule that functionally mimics the role of the antenna in NPQ is described. When the hexad is dissolved in an organic solvent, five zinc porphyrin antenna moieties absorb light, exchange excitation energy, and ultimately decay by normal photophysical processes.

However, when acid is added, a pH-sensitive dye moiety is converted to a form that rapidly quenches the first excited singlet states of all five porphyrins, converting the excitation energy to heat and rendering the porphyrins kinetically incompetent to perform useful photochemistry.

Charge transport was also studied in single-molecule junctions formed with a 1,7-pyrrolidine-substituted 3,4,9,10-Perylenetetracarboxylic diimide (PTCDI) molecule. A reduction in the highest occupied (HOMO) and lowest unoccupied (LUMO) molecular orbitals energy gap due to the electronic properties of the substituents is seen when compared to an unsubstituted-PTCDI. The small HOMO-LUMO energy gap allows for switching between electron- and hole-dominated charge transport with a gate voltage, thus demonstrating a single-molecule ambipolar field effect transistor.

To my parents for nurturing my curiosity,
and to my grandparents for endless support.

ACKNOWLEDGMENTS

While there are many people that I must thank for helping me through my graduate career, I have to start with my advisors, Tom Moore, Ana Moore and Devens Gust. Your patience, guidance, wisdom and experience have been undoubtedly influential, not only to my scientific career, but my personal life as well. Your variety of perspectives have always kept me in check and provided me with another point of view for whatever situation I may find for myself. You have afforded me the opportunity to delve into the deepest realms of science and to see the world while doing it. For all of this, I am forever indebted. It has truly been a privilege to spend this time in your laboratory and learn from you.

A special thanks to Mike Hambourger for not only getting me started with hydrogenase, but also being a friend and helping me along the way, answering stupid questions and always being up for a beer…even at 9:00 am. You taught me not just electrochemistry, but how to be a respectful scientist in general. I am truly grateful for the knowledge that I have gained from you. I also must thank Jeff Crisman, Jesse Bergkamp, Ben Sherman and Michael Vaughn for being the greatest friends one could ask for and for your unending support and help in the lab. Between the four of you, any question can be answered and much fun can be had. Thanks to all the current and former members of the Gust, Moore, Moore group.

I also must thank Paul Liddell, Yuichi Terazono, Matthieu Koepf and Julien Frey for being a positive influence in my life and providing a friendly work environment. Thanks to Isma Díez-Pérez, Josh Hihath, Chris Bruot and all of the

folks in Dr. Tao's lab for providing a different perspective and much help with STM experiments. As a wise physicist once told me, why climb a mountain, all you gain is potential energy ;-) Thanks to Christina Minniti for your help in the lab and for providing a much more artistic perspective than I have myself. I also need to express some gratitude to Science Foundation Arizona for my financial support as well as affording me the opportunity to study here and attend meetings. Thanks to my collaborators Paul King, Maria Ghirardi, Kate Brown and David Mulder from the National Renewable Energy Laboratory for fruitful discussions and an endless supply of hydrogenase.

Thanks to my parents for unending support and encouragement while providing an extremely unscientific point of view. You supported me through many explosions in the house and never asked questions. A special thanks to my grandparents, George and Dorothy, who unfortunately aren't here to see me graduate. You always showed interest, even when I know you had no idea what I was talking about and have supported me along the way. Thank you for your encouragement.

An extremely special thanks to Jim Bridgewater and Verina Kranak for your friendship and endless support and perspective. I learned more living with the two of you than during any other time in my life. I realized that life is too short to take anything for granted and that I should enjoy what I have and push myself to do what I am truly capable of. It is from the two of you that I really learned how to live life to the fullest. Thank you both for everything; you have my everlasting gratitude and friendship.

TABLE OF CONTENTS

Page

CHAPTER Page

LIST OF FIGURES

CHAPTER 1

BACKGROUND

1.1 Significance

As the world's demand for energy increases, it is more important than ever to develop an economy that is carbon-neutral and utilizes sustainable technologies. Human demand for energy is projected to increase drastically over the next ~20 years, so it is ever more important to secure an economy run with sustainable practices. Sunlight is the ultimate source of energy for the majority of life on Earth with the amount of solar energy hitting the Earth's surface far surpassing current human demands; however, direct conversion of sunlight to a useable fuel remains a formidable challenge.[1] Photosynthesis is the natural process by which organisms convert solar energy into stored chemical energy in the form of sugars. The ability to utilize only photons to catalyze the thermodynamically uphill conversion of water to hydrogen (H_2), releasing only molecular oxygen (O_2) as a by-product, has yet to be achieved. Solar energy conversion to electricity, while attainable at moderate efficiencies, has the drawback of only being possible during the day; a solar to fuel conversion system could overcome this by storing the energy of the sun for use during the night or periods of reduced light. Hydrogen production directly from sunlight, utilizing only fully renewable resources such as water and photons, is an ideal solution, and newly developed materials and techniques show promise for solar hydrogen production,[2,3] although no cost-effective solution to the problem has been identified. Biological systems for the conversion of sunlight to hydrogen are of particular interest because

Nature has already solved the problems that scientists now face. However, utilizing biological systems for technological purposes introduces new problems and challenges. Hydrogen has the benefit of being very versatile. It can be used directly in both an internal combustion engine and a fuel cell. Hydrogen is the most abundant element on Earth and is also an efficient energy carrier, although only a small fraction is found as useable molecular hydrogen (H_2).[4] Hydrogen is used as a fuel, or rather an energy carrier, in both biological systems and technological systems and has proven useful for a variety of energy-based applications, most commonly in fuel cells.[5] A hydrogen-based economy can be both carbon-neutral and sustainable if executed properly; however, the vast majority of commercially produced hydrogen today is obtained through steam reformation of natural gas or other energy intensive processes.[6] Other common methods of producing hydrogen include the electrolysis of water via electrolyzers that utilize precious metals such as platinum and the thermochemical splitting of water which requires large energy inputs; neither of these approaches are practical for sustainable, large-scale hydrogen production.[7] Thus, another means of hydrogen production is necessary.

1.2 Catalysts

Effective and efficient catalysts are at the heart of energy related research from both a technological and a biological perspective as they produce the desired fuel product and decrease the amount of energy required to reach that product. The chemical processes related to solar energy conversion to a fuel such as water oxidation and proton reduction largely rely upon catalysts composed of rare or

noble metals to carry out the desired reactions, which of course is not a sustainable practice. The limited quantity of such metals makes them unviable for large scale, sustainable use, although many current systems such as electrolyzers and fuel cells currently incorporate precious metals. Biological catalysts on the other hand, utilize solely earth abundant metals to perform complex reactions, such as splitting water. A substantial body of published work explores how to mimic biology for technological purposes, arguably the most important work being directed towards water oxidation catalysts.[8-11]

Several issues must be addressed before large-scale utilization of hydrogen as a fuel can be implemented. The energy density of hydrogen is low compared to that of carbon-based liquid fuels and it is difficult to store and transport efficiently.[6] On site hydrogen production could be used to overcome transportation problems, although storage remains an issue. Alternatively, solar energy may be used to reduce carbon dioxide (CO_2) in a multi electron reaction to a useable fuel such as formate, methanol, methane or sugars. Thermodynamically all of these reactions occur at approximately the same potential, (close to that of the H^+/H_2 couple at -413 mV vs. NHE at pH 7) but the kinetics are typically slow and up to 24 electrons are required to produce the final fuel product. Overpotential requirements for these reactions are also large, requiring up to several hundred millivolts to drive the reaction. Despite these obstacles, progress is being made in the development of new catalysts for the production of carbon fuels.[12,13] The reduction of CO_2 to a useable fuel is a viable alternative to hydrogen production for the conversion of solar energy to chemical bonds. The

production of a liquid fuel with a high energy density using only base metals for catalysis has the potential to change the basis upon which our society functions. However, due to the complexity of reducing CO_2 to a useable fuel, hydrogen is a good target for first generation solar fuel conversion systems.

1.3 Single Molecule Techniques

1.3.1 Scanning Tunneling Microscopy (STM)

The invention of the scanning tunneling microscope (STM) by Binnig and Rohrer in 1981 marked a new era for science with the ability to image surfaces on the subatomic level. Their discovery led to the Nobel Prize in Physics in 1986 and has proven influential to nearly every discipline in the physical sciences. Not only can this device be used to image a surface, it can also manipulate single atoms and, with some tuning, it can be used to measure the electronic properties of single molecules. The following discussion will go through the theory of operation and some of the many uses of this microscope as well as some of the current research in the field.

The STM operates on the concept of quantum mechanical tunneling, whereby electrons are able to tunnel through space from one electrode (i.e. the tip) to another (i.e. a substrate).[14] In a typical STM setup, a tip made of a metal (commonly platinum, gold or tungsten) is brought into close contact with a conductive substrate. A voltage is applied to each of the electrodes resulting in electron tunneling, termed a tunneling current, when the electrodes are brought into close contact with one another. The resulting tunneling current is a product of many variables such as the tip position, the conductivity of the sample on the

substrate and the applied voltage. Typically, STM data is presented as an image although the actual data is a current that maps the conductivity of a surface. For imaging a conductive surface, the resolution of a STM is roughly 0.1 nm laterally and 0.01nm in the z direction, hard to match with any other technique.[15] To achieve such high resolution, the entire STM apparatus must remain very stable throughout the duration of an experiment. Active anti-vibration tables that utilize piezoelectrics are commonly employed to maintain a level of stability sufficient for high resolution imaging. Other simpler methods to isolate vibrations and other forms of noise from the STM setup will be discussed in more detail in chapter 5.

1.3.2 STM Configurations and Considerations

STM can operate in a variety of media such as vacuum, air and liquids. As described above, STM uses two electrodes with a bias applied between them for imaging in a simple two electrode setup. This works while operating under vacuum and in air where the medium is nonconductive. When a conductive medium such as water or an organic solvent containing a supporting electrolyte is used, a potentiostat and electrochemical setup must be employed in conjunction with the typical STM setup. When this is done, the technique is referred to as electrochemical STM (EC-STM), and the setup is further complicated by the necessity for reference and counter electrodes in the circuit, thus necessitating a bipotentiostat with the ability to control two working electrodes. By adding a reference electrode, a known potential can be applied to each electrode and thus the bias of a known potential is acquired. In solution, the tip must be insulated to prevent large current flow arising from operating in a conductive medium. This

current is referred to as a leakage current and prevents effective imaging of the sample and data acquisition. Thus, STM tips are coated with insulating wax or other substance. Typical tip coatings are Apiezon wax and polymers such as polyethylene. When applied to an STM tip, they insulate all but the very end allowing only a limited electrode area for tunneling. Another very effective method for tip insulation is to electropolymerize an insulating monomer directly onto the tip surface. This technique has been elegantly demonstrated by Díez-Pérez *et al.* and has proven useful for a variety of tip metals and configurations.[16] Without effective tip insulation methods, EC-STM would not be possible. The ability to work in solution and image on the sub-nanometer scale has made STM the technique of choice for many measurements, including many in this dissertation.

1.4 Summary

Over the past 20+ years, a considerable body of work surrounding alternative energy and artificial photosynthesis has developed. From synthetic organic systems that mimic portions of natural photosynthesis to systems relying on the prowess of biological catalysts, much knowledge has been gained in the field and great progress continues to be made. The development of robust systems for the conversion of solar energy to fuel remains a goal of researchers. Utilizing biological components such as hydrogenases has shown promise for the interconversion of protons and molecular hydrogen in such systems. STM, when combined with electrochemical techniques, can provide much information about complex systems that a single technique alone cannot. The following chapters will

describe, in detail, research related to these fields performed during the duration of this degree.

CHAPTER 2

HYDROGENASE TECHNIQUES

2.1 Introduction

Hydrogenases are of growing interest due to their utilization of common metals at their active sites and ability to catalyze the $2H^+ + 2e^- \leftrightarrows H_2$ redox system under nearly activationless conditions, with concomitant energy storage or release.[17-21] They serve as models for catalysis of this most fundamental of redox reactions. Interest in the catalytic abilities of hydrogenases for hydrogen generation has led to various electrochemical studies[22-25] as well as photoelectrochemical hydrogen production studies.[26]

A typical [FeFe]-hydrogenase is *Ca*HydA, a 65.4 kD protein with a highly conserved [6Fe-6S] catalytic H-cluster as well as three [4Fe-4S] and one [2Fe-2S] accessory clusters. The proximity of the distal [FeS] cluster to the exterior of the protein allows electrons to be transferred directly from an external redox partner, presumably through a chain of [FeS] clusters, to the H-cluster, where catalysis occurs and hydrogen is produced or oxidized.

Direct electrochemical measurement of catalytic currents on macroscopic electrodes as a function of applied potential has yielded valuable information.[20] The *Ca*HydA [FeFe]-hydrogenase, as well as other [FeFe]-hydrogenases, reportedly show a preference for proton reduction over hydrogen oxidation,[21] leading them to be investigated as a means of producing hydrogen. On the other hand, hydrogenases biased towards hydrogen oxidation could serve as catalysts in fuel cells.[27] The mechanism of bias in either hydrogen oxidation or proton

reduction is not clear: electrochemical studies have shown that these catalysts appear to operate very near the prevailing thermodynamic potential of the H^+/H_2 couple and therefore cannot differentially favor the reduction or oxidation.

Numerous electrochemical studies with both [NiFe] and [FeFe]-hydrogenases have been performed at carbon electrodes,[24,26,28-32] while a handful have been performed on gold and modified gold electrodes.[33,34] Although most studies utilize hydrogenase adsorbed on an electrode as an ensemble average of orientations,[35] attempts have been made to specifically orient the protein on the electrode surface.[36,37] A suitably oriented molecule allows for better defined interfacial electron transfer[38] and the possibility of observing the largest current densities attainable for a given system. Maximum current densities are necessary to observe maximum turnover, and the number of molecules participating in the reaction must be known in order to calculate the turnover frequency (TOF). Previously, surface coverage of hydrogenases on electrodes was either estimated based on the electroactive surface area of an electrode, or by inhibiting the enzyme to reveal non-turnover signals from redox cofactors inside the protein.[39,40] While the latter technique can be useful and has provided the first measurements of electroactive surface coverage, it has only been demonstrated in a limited number of cases with specific hydrogenases, most notably a [NiFe]-hydrogenase from *Allochromatium vinosum*.[41] Calculation of the electroactive surface coverage of enzyme enabled Armstrong *et al.*, to calculate accurate TOFs for various hydrogenases.[23,27] One study has also shown that a [NiFe]-hydrogenase from *Thiocapsa roseopersicina* can be imaged with a scanning tunneling microscope in

a Langmuir-Blodgett film; I-V curves of the protein film were reported.[42] The ability to measure redox processes of simple proteins through SAMs has also been investigated previously where one-electron oxidations and reductions were taking place.[43] More complicated, multi-electron or catalytic processes have also been measured through SAMs. However those studies did not involve the use of single-molecule topographic techniques such as STM to determine surface concentrations.[33,44] Knowing the actual surface coverage on an atomically flat surface is crucial to accurately calculate the catalytic TOF, measured as a function of applied potential, per single adsorbed enzyme molecule.

The measurement of the maximum TOF of hydrogenase molecules is the most direct indication of catalytic prowess. Such a measurement requires accurate knowledge of the concentration of active protein and of substrates and products. However, performing this measurement in solution remains a formidable challenge because saturating concentrations for both substrates cannot be realized. Varying the substrate (H^+) concentration as necessary to allow for a typical biochemical assay to determine the turnover of the hydrogenase is not possible because the protein is rendered inactive outside a narrow pH range.[26,45,46]

In this study, the enzymatic turnover of an [FeFe]-hydrogenase, *Ca*HydA from *Clostridium acetobutylicum*, was investigated which is homologous (70% identity)[47] with the [FeFe]-hydrogenase from *Clostridium pasteurianum*, CpI, for which structural data exists.[48,49] The *CaH*ydA was chosen for this study due to its high catalytic activity for hydrogen production and the relative ease of recombinant expression.[47] The enzyme was adsorbed onto a negatively charged,

self-assembled monolayer (SAM) on a flat gold surface for investigation by electrochemical scanning tunneling microscopy (EC-STM) techniques and macroscopic electrochemical measurements. The EC-STM imaging allowed quantitative determination of the number of bound enzyme molecules. The bound enzymes were catalytically active, and cyclic voltammetry (CV) yielded a characteristic cathodic hydrogen production signal when the potential was scanned sufficiently negative. The quantitative determination of the enzyme distribution on the Au-SAM surface coupled with macroscopic electrochemical measurements obtained from the same electrode allowed the evaluation of a TOF as a function of potential for single [FeFe]-hydrogenase molecules.

2.2 Experimental

Electrochemical scanning tunneling microscopy (EC-STM) studies were performed with a Pico-SPM (Agilent, AZ) using a Nanoscope E controller and a bipotentiostat (Agilent, AZ). Imaging experiments were performed in a homemade Teflon cell using as a working electrode an atomically flat Au (111) substrate prepared by thermally evaporating ~130 nm of gold (Alfa Aesar 99.999 %) onto freshly cleaved mica surfaces under ultra high vacuum (~2 x 10-8 torr). The STM tips were prepared by mechanically shearing Pt/Ir wire (80/20, 0.25 mm diameter) and coating the tips with Apiezon wax. All tips had <1 pA leakage current, the tunneling current set point was 200-400 pA with a 10 nA/V current amplifier and a 100 mV sample bias was typically applied. All Au (111) substrates were annealed with a hydrogen flame prior to use and subsequently immersed in ethanolic solutions of mercapto-carboxylic acids to form self-

assembled monolayers (SAMs). The resulting SAMs were imaged without protein to ensure formation of the SAM and cleanliness of the surface. The *Ca*HydA was subsequently adsorbed in-situ to the monolayer with 0.1 M phosphate buffer, pH 7.0, as the supporting electrolyte and imaged in EC-STM mode to control substrate potential. All EC-STM images were recorded with a substrate potential of -400 mV vs. Ag/AgCl. Titration of protein to control surface coverage results in the adsorption of protein to the modified gold surface over the course of several minutes to a few hours to reach equilibrium.

The [FeFe]-hydrogenase *Ca*HydA from *Clostridium acetobutylicum* was purified and expressed in *Escherichia coli* (*E. coli*) and assayed for H_2 evolution activity according to previously reported procedures.[50] Due to the extreme oxygen sensitivity of [FeFe]-hydrogenases,[25,51,52] all work was performed in an anaerobic chamber (Coy Laboratory Products) under strictly anaerobic conditions (2-3 % H_2, bulk N_2, <1 ppm O_2). Under anaerobic conditions and at ambient temperature (~25° C), *Ca*HydA is stable for several hours in the electrochemical STM setup with little or no observed loss in electrocatalytic activity.

All hydrogenase samples used for the experiments presented in this dissertation were prepared by collaborators at the Biosciences Center of the National Renewable Energy Laboratory (NREL) in Golden, Colorado. Recombinantly expressed *Ca*HydA was isolated and purified by Kate Brown, David Mulder or Paul King of NREL and shipped to ASU overnight, on ice, to ensure activity was retained and sample degradation did not occur. In short, *Ca*HydA was expressed in *E. coli* and purified according to previously reported

procedures.[47] Due to the extreme oxygen sensitivity of this particular hydrogenase, purification was performed under strictly anaerobic conditions.[25,51,52] Storage and shipment of purified enzyme was also conducted under anaerobic conditions to prevent inactivation of the enzyme. Purified hydrogenase could be stored for months under anaerobic conditions at 4°C in a buffer consisting of 50 mM Tris, 5 mM NaCl, 5 mM sodium dithionite and 5% (v/v) glycerol. The presented work utilizes solely enzyme purified by collaborators and kept under a nitrogen/hydrogen atmosphere in the buffer conditions described above.

Prior to electrochemical experiments all enzyme samples were assayed for activity using sodium dithionite and methyl viologen in a technique adapted from the literature.[47,50] A typical assay involves 100 mM sodium phosphate buffer (pH 7.0), methyl viologen (100 mM in 100 mM sodium phosphate buffer, pH 7.0) and sodium dithionite (100 mM) in 30 mM sodium hydroxide. Solutions were made anaerobic prior to use either by argon bubbling at least 30 min in a septum sealed vial or by exposure to a glovebox atmosphere (2-3% H_2, bulk N_2) for several days. To perform the assay, 870 μL sodium phosphate buffer, pH 7.0, was added to a 7.5 mL vial inside the glovebox. To this vial was added 50 μL of 100 mM methyl viologen in the same buffer and 5 μL purified hydrogenase. The vial was sealed with a septum, removed from the glovebox and placed on ice in a covered container. The headspace of the septum sealed vial was then flushed with argon for 30 min to remove hydrogen in the vial arising from the glovebox atmosphere. At the same time, 30 mM sodium hydroxide was bubbled with argon in a 7.5 mL

septum sealed vial for at least 30 min, followed by the addition of sodium dithionite to 100 mM and an additional 30 min of argon bubbling. To initiate the assay, 75 µL sodium dithionite solution was added to the vial containing the hydrogenase and placed in a water bath at 37° C for 15 min. Subsequently, a 500 µL sample of gas from the headspace was removed with an airtight syringe (Hamilton #1001) and analyzed via gas chromatography for hydrogen. A gas standard (1% H_2, bulk N_2) was used to calibrate the gas chromatograph to ±10 % of the measured value prior to each activity assay. A 5 Å molecular sieve column was used in conjunction with a thermal conductivity detector (TCD) with ultra high purity Argon as a carrier gas. Peak Simple software was used to record data from a SRI Instruments Model 310 gas chromatograph. In most cases, the assay was repeated with two or three samples to ensure accuracy. A quantitative measurement of hydrogen was obtained from gas chromatography as mol % hydrogen in the headspace gas. This value can be used to calculate the activity of the hydrogenase sample in µmol H_2 produced min^{-1} mg^{-1} protein, referred to as activity units (U). Typical results of activity were 3 to 1500 U depending on the preparation, with later preparations having a significantly higher specific activity due to modifications of the expression/purification procedures. This study used two separate *Ca*HydA preparations with nominal solution-based specific activities for H_2 production of 177 and 280 U, which correspond to solution based TOFs of 192 s^{-1} and 303 s^{-1} respectively. All data were normalized to both the surface coverage of protein and the specific activity.

Cyclic voltammetry was performed with a CH Instruments 650C electrochemical workstation using a platinum wire counter electrode and either a silver wire quasi reference or a silver/silver chloride reference electrode. The Au (111) substrate modified with a carboxylate-terminated SAM was used as a working electrode. All CVs were performed in the same EC-STM cell, with a geometric surface area of 0.283 cm^2. The same sample was used for imaging by EC-STM inside an anaerobic chamber as well as anaerobic CV in a typical three-electrode configuration. All CVs were recorded in 0.1 M phosphate at pH 7.0 with a scan rate of 50 mV/s.

STM images were scrutinized by eye to estimate the number of proteins on the surface. Several 100 nm by 100 nm images from different areas of the electrode were analyzed, particles were counted and an average coverage was obtained, which was then used to estimate the number of proteins on the geometric surface. Variation in surface coverage among images was <10 % for a given sample. To verify the methodology of counting individual particles in order to quantify enzymes on the electrode, two of the STM image-quantified samples were tested for iron content via a ferrozine iron binding assay adapted from previously reported procedures.[53,54] The quantity of iron determined by this procedure differed from that determined by counting the images by 50% to 20% underestimation, indicating that qualitatively the method of counting the images is valid. Due to the minute amounts of protein in the experiments, (~10^{-12} mol of protein/cm^2), the difficulty of recovering protein from surfaces, and detection limitations by UV-Vis absorption measurements, data from the STM images

alone were used to calculate a TOF in this report. Recovered samples were also analyzed by SDS-PAGE to confirm that the molecular weight of the adsorbed protein was consistent with *Ca*HydA.

As a complement to the STM images, additional measures were taken to ensure the identity and quantity of *Ca*HydA on the surfaces. To confirm the identity of the protein adsorbed to the surface, SDS-PAGE was run with samples recovered from the Au (111) substrates used for STM imaging experiments against purified *Ca*HydA. Protein samples were recovered from STM substrates with a sample solubilization buffer consisting of Tris (150 mM), glycerol (30% v/v), 2-mercaptoethanol (6% v/v), sodium dodecyl sulfate (12% w/v) and coomassie brilliant blue G-250 (0.05% w/v) or by subjecting the samples to a high concentration of salt (~0.5 M) to disrupt the electrostatic interaction between SAM and protein. The resulting sample containing solution was recovered from the substrate and run with SDS-PAGE against pure, soluble protein as received by collaborators at NREL. Matching bands were observed at ~65 kD (see Figure 6), confirming the identity of the protein on the surface. The detection of such a small amount of protein was difficult and at the limit of detection for this technique[55-57] so three Au (III) substrate samples were used to gather a sufficient quantity of protein to detect. The amount of protein detected was, however, also consistent with calculations of protein quantity from the STM images.

As an independent estimate of the amount the *Ca*HydA adsorbed to the STM substrate, samples were recovered under denaturing acidic conditions, and the Fe was quantified using a modified ferrozine assay adapted from literature

procedures.[53,54] Although this assay was near its limit of detection, the amount of Fe observed was also qualitatively consistent with the STM imaging results. *Ca*HydA incorporates 20 iron atoms into cofactors in its structure, allowing for protein quantification via iron quantification. A standard curve from ferrous chloride was used to calibrate the quantity of iron from the recovered protein samples.

A homology model of the *Ca*HydA [FeFe]-hydrogenase was also constructed from alignment with 1FEH in the PDB database using modeler and was constructed using the salign command[58] within modeler by Michael Vaughn in the laboratory. This model was used exclusively for this work and is very similar to the 1FEH structure, which is the *Clostridium pasteurianum* structure, as it shares 70% sequence identity.[47] Electrostatic surface potentials were generated using the PBEQ web server using default settings[59,60] and visualized in VMD[61] with +1kcal/(mol e^-) isosurface in blue the -1kcal/(mol e^-) isosurface in red. These models are depicted in Figure 1, where the electrostatic surface of the protein is shown to interact with the negative charge of the SAM.

2.3 Results

2.3.1 Assembly on SAMs

SAMs were prepared on atomically flat gold electrodes with carboxylic-acid terminated alkanethiols. The acid moieties, which are negatively charged at the pH of these experiments, are designed to interact with the large regions of positive charge that are present on the protein surface. Ideally, such interactions are both strong and serve to orient the enzyme molecules all with the same face towards

the gold. We employed SAMs having three to eleven carbon atoms in order to alter the distance between the protein and the electrode surface. Figure 1a-c depicts the proposed interaction between the positively-charged protein surface and the negatively-charged monolayer surface based on electrostatic considerations.[62]

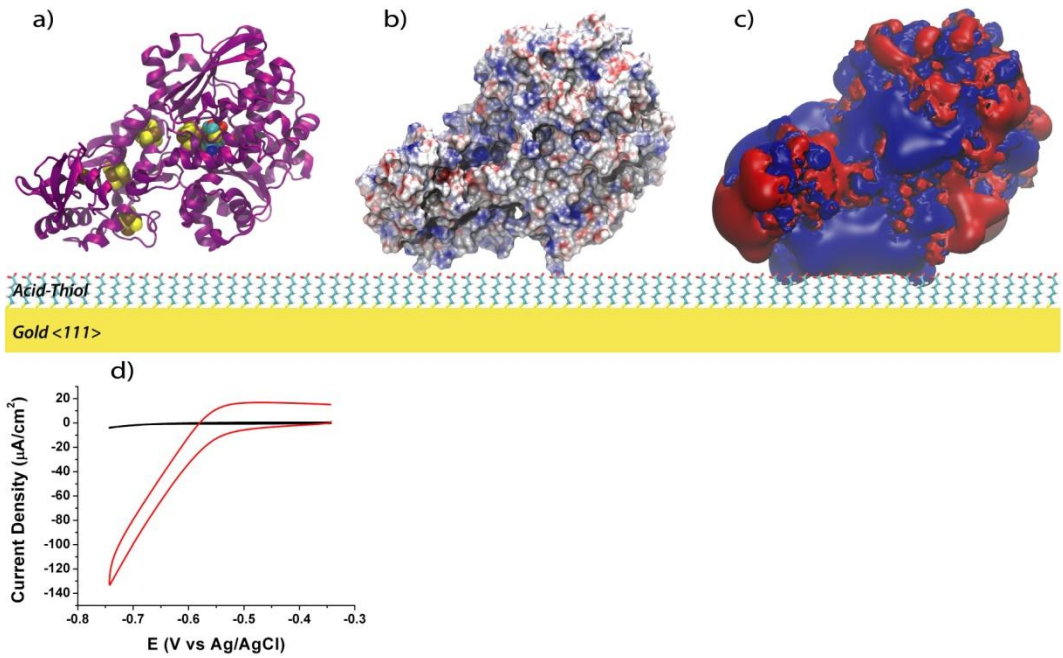

Figure 1. (a) Homology model of *Ca*HydA [FeFe]-hydrogenase on a 6-mercaptohexanoic acid-modified gold electrode. Panels a-c are shown for identical orientations. (b) Electrostatic surface potential of homology model of *Ca*HydA on negatively charged SAM surface. (c) Isopotential surfaces generated by *Ca*HydA. The +1 kcal/(mol · e) surface is depicted in blue, and the -1 kcal/(mol · e) surface is depicted in red. The orientation depicted in this panel maximizes the positive surface exposure to the carboxylates of the SAM, although other orientations are possible. (b, c) electrostatic calculations were performed at neutral pH and room temperature (25 ºC). (d) Typical cyclic voltammogram of *Ca*HydA on a 6-mercaptohexanoic acid-modified gold electrode. The black scan is a blank of the 6-mercaptohexanoic acid-modified electrode. The red scan depicts *Ca*HydA adsorbed to the SAM.

Although, the relative energies of this orientation and others were not rigorously calculated; the area of exposed positive charge of *Ca*HydA interacting with the carboxylated surface of the SAM is maximized in these structures. Recently, Brown *et al.* have shown that CdTe nanocrystals capped with 3-mercaptopropionic acid interact with a region of positive charge on the surface of *Ca*HydA to form a stable complex for the photoproduction of hydrogen.[63] Our system presumably utilizes the same region of positive charge, which surrounds the proposed binding site for the negatively charged ferredoxin during in vivo electron transfer.[47] This is the point where electrons are thought to enter the *Ca*HydA electron transfer chain. Cyclic voltammetric studies were performed on these Au-SAM electrodes with bound *Ca*HydA and large catalytic electrochemical signals for hydrogen production were observed (Figure 1d), suggesting that the orientation of the protein on the electrode is favorable for electron transfer (ET).

2.3.2 EC-STM

EC-STM was chosen for imaging in this work for its ability to provide high resolution imaging in a liquid medium as well as potentiostatic control of both tip and substrate. With *Ca*HydA stably adsorbed onto carboxylate terminated SAMs, the resulting surface was imaged, revealing random, relatively uniform coverage (Figure 2a-d). The electrochemical signal (Figure 1d) on the Au-SAM electrodes resembles that on PGE electrodes,[26] both in observed current density for short carbon chains, and waveform. It has been previously demonstrated that under conditions like these, hydrogenase molecules free in solution do not contribute

significantly to the catalytic current.[46,64] This suggests that the enzyme-surface interaction is stable, and that the catalytic current can be ascribed to the enzyme molecules detected in the STM images.

The apparent height of the protein on the surface reflects the magnitude of the current flowing through the enzyme between the tip and gold substrate. This current changes with substrate potential (EC-STM) due to the properties of the redox active cofactors incorporated in the protein, specifically the distal [FeS] cluster which serves as an initial acceptor for intramolecular ET. As the substrate potential is shifted negative, the Fermi levels of both working electrodes (i.e., the tip and substrate) will bracket the redox level of the protein, at some point meeting resonant tunneling conditions and giving rise to an increase in the tunneling current through the protein. A higher current is observed at roughly -0.6 V vs. Ag/AgCl, the potential at which proton reduction occurs, which is closely matched to the redox properties of the [FeS] clusters. Under these conditions, topographical STM images show larger apparent heights for the redox active hydrogenase (see Figure 2b-d). When the Fermi levels of the electrodes are positive or negative of the midpoint of the redox center (i.e. non-resonant tunneling conditions), the height appears smaller due to the decreased protein conductivity. Theoretically this observation should give a Gaussian distribution of heights versus substrate potential as the potential is swept past the midpoint of the redox center. This phenomenon has been recorded previously for redox proteins such as azurin[65] as well as other redox-active small molecules.[66] In our case, only

one side of the curve can be observed due to limits imposed by solvent reduction at the tip at increasingly negative potentials.

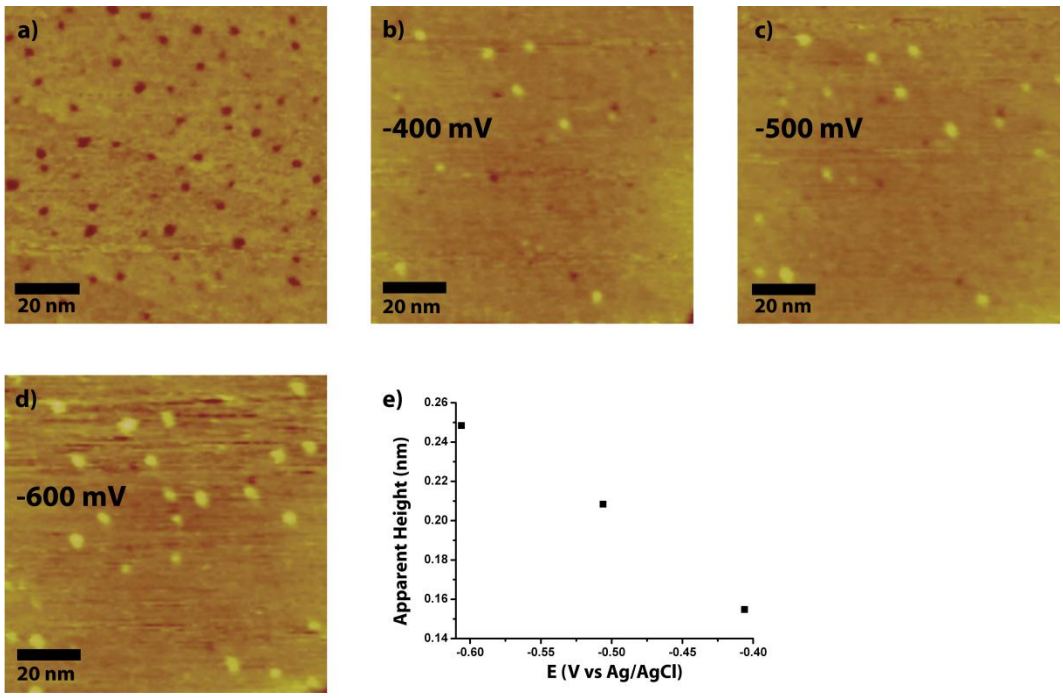

Figure 2. (a) EC-STM image of a 3-mercaptopropionic acid/ethanethiol SAM (1:1) on a Au (111) surface without protein; E_{bias} = 200 mV, i_t = 400 pA. (b-d) CaHydA adsorbed onto the modified surface at substrate potentials ranging from -400 mV to -600 mV vs Ag/AgCl. The images show an increasing apparent height with increasingly negative potentials. (e) Graph showing the apparent height of *Ca*HydA as a function of potential.

2.3.3 Cyclic Voltammetry

The overall electrochemical properties of such electrodes may be studied using standard cyclic voltammetric techniques. A catalytic hydrogen production current due to enzymatic turnover is observed when sufficient driving force is applied to the electrode as seen in Figure 3. For accurately measuring these currents, samples with high density surface coverage (0.5-2 pmol/cm^2) were prepared as seen in the inset of Figure 3. The observed catalytic current is directly related to the amount of hydrogen produced from the enzyme. Taken together, the catalytic current and surface coverage were used for the calculation of a TOF per adsorbed *Ca*HydA.

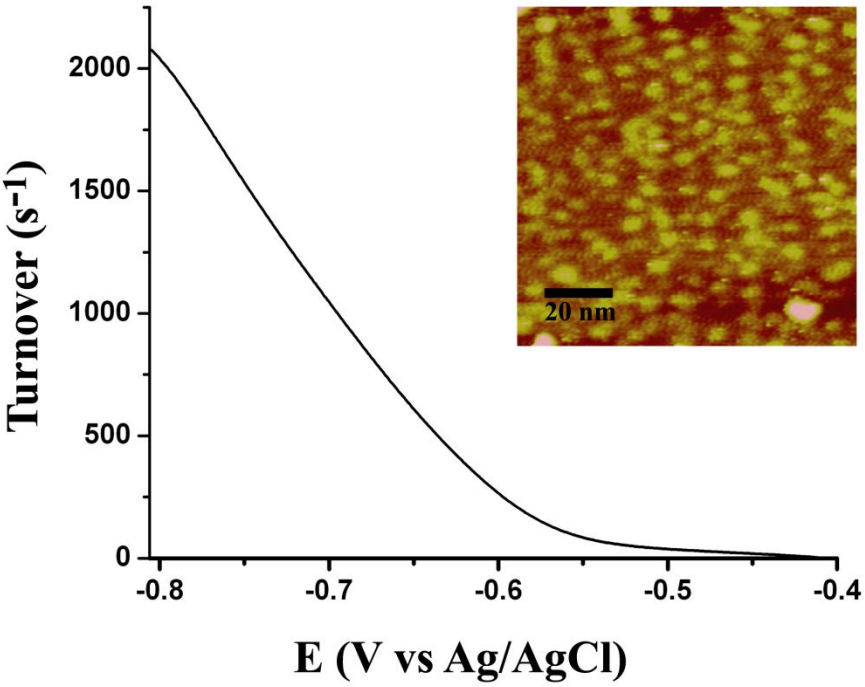

FIGURE 3. Turnover of a high surface coverage *Ca*HydA electrode plotted as a function of potential. (Inset) STM image of the same electrode. Combining the electrochemical data and protein coverage from the inset allows for calculation of a turnover frequency per adsorbed protein molecule.

The distance between the electrode and enzyme was altered by varying the SAM alkyl chain length from three to eleven carbons. As a result, the current densities at a given voltage declined exponentially with increasing SAM length. Figure 4 depicts typical CVs of *Ca*HydA on Au-SAM electrodes of lengths from three to eleven carbons, showing a decreasing catalytic current (i.e. turnover) for increasing chain length.

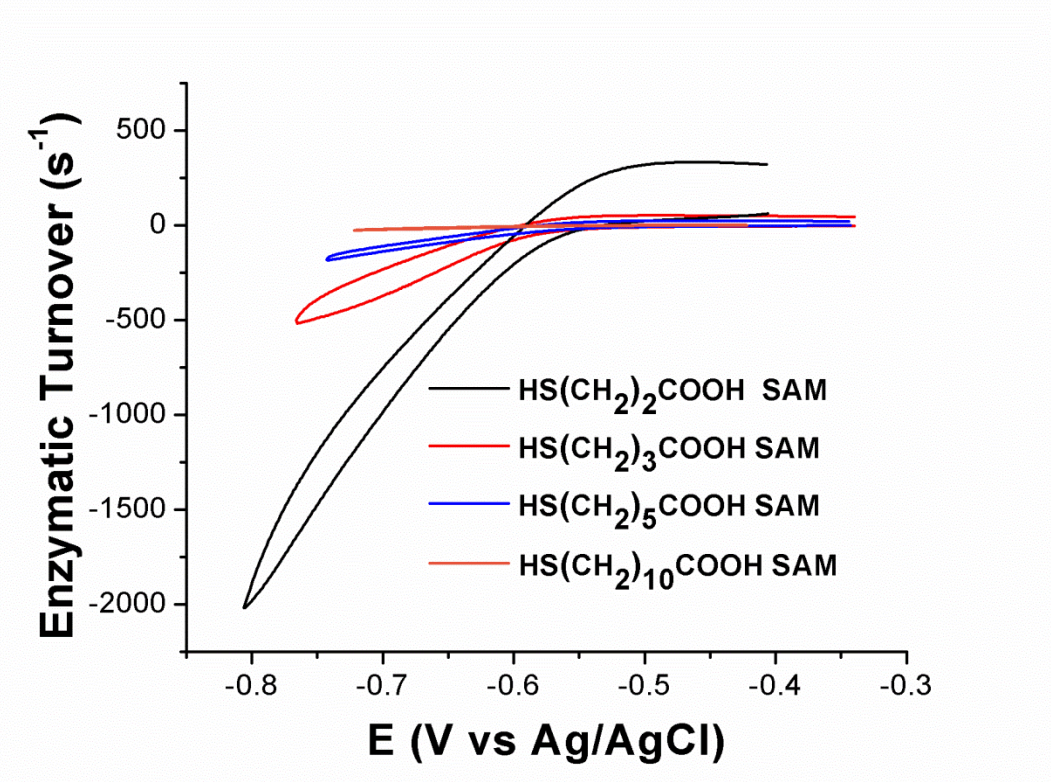

FIGURE 4. Enzymatic turnover of *Ca*HydA as a function of applied potential recorded on different lengths of carboxylate-terminated SAMs.

2.4 Discussion

From the catalytic hydrogen production current recorded through SAMs of various lengths and the number of enzyme molecules per electrode area counted from the STM images of each electrode, a TOF per molecule of *Ca*HydA can be calculated at any given applied potential. The TOF per protein at -0.7 V was plotted as a function of SAM length and fitted to an exponential decay function (Figure 5) according to eq. 1, where *i* is the tunnel current at a distance d from the electrode, i_0 is the limiting current in the absence of the SAM layer, and β is the electronic decay constant.

$$i = i_0 e^{-\beta d} \quad (1)$$

An incremental distance per carbon in the alkyl chain of 1.25 Å was calculated based on 109.5° carbon-carbon bond angles and a carbon-carbon bond length of 1.54 Å. From this, the length of the SAM alkyl chain and estimated the distance (d) through which electron transfer between the enzyme surface and the electrode must occur was calculated. The experimental electronic decay constant was determined to be 0.82 ± 0.16 $Å^{-1}$. This agrees well with values reported in the literature for self-assembled monolayers of alkanethiols and is consistent with values obtained from drastically different techniques, including single-molecule junction measurements.[67] The exponential decay behavior is a consequence of control of the catalytic rate by ET through the SAM to the protein. ET through the protein itself to the catalytic site is the same for all SAM-protein constructs and, we conclude, does not control the catalytic rate at the potentials investigated.

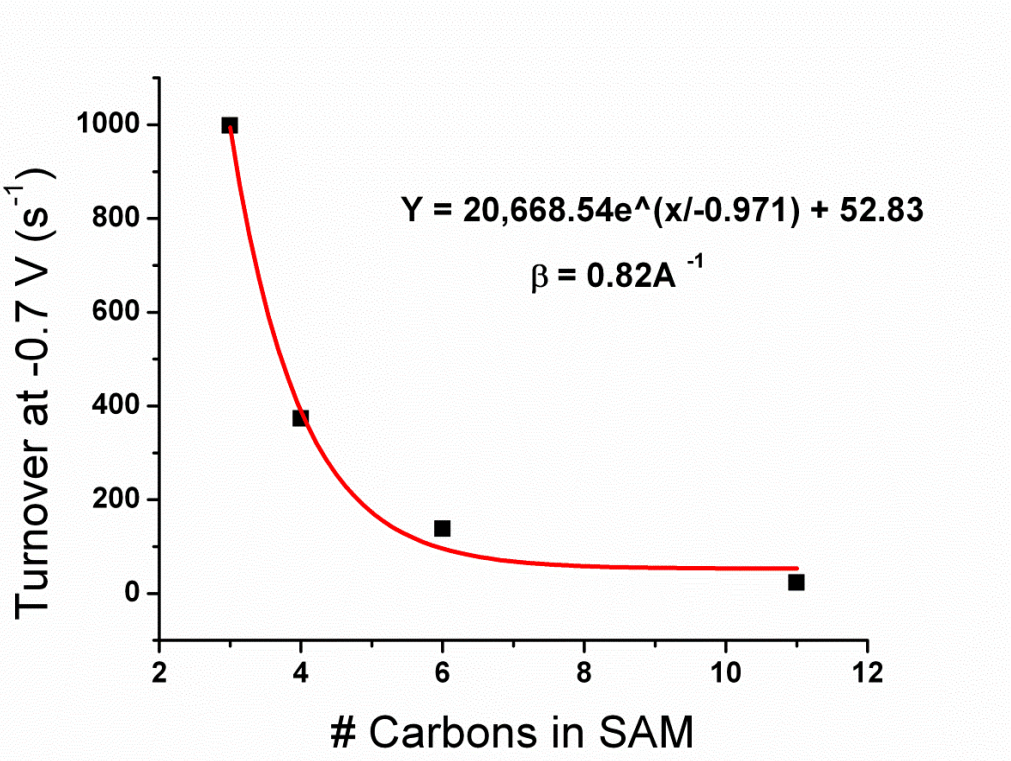

FIGURE 5. Single-protein turnover as a function of number of carbons in the SAM fit to an exponential function to extract the electronic decay constant.

Extrapolation of this plot to a distance of zero, approximating a *Ca*HydA molecule in direct contact with the bare gold electrode surface where eq. 1 simplifies to $i = i_0$, gave a TOF of ~21,000 ± 12,000 s^{-1} at pH 7.0, which is higher than previous estimates in the literature for hydrogenases.[27,44,45] Methods using non-turnover signals for estimates of protein coverage have given a TOF upwards of 10,000 s^{-1}.[20] Catalytic current normalized by STM-derived surface density thus provides an average of the TOF for individual enzyme molecules for any given potential within the window of the electrochemical signal for *Ca*HydA. This number does not account for inactive protein at the electrode interface or enzymes in an orientation unfavorable for interfacial ET and is thus a lower limit for turnover.

The electrochemical signal observed in cyclic voltammetry and the potential at which proton reduction occurs agree well with those reported in the literature for various electrode surfaces,[26,33,36] confirming that the kinetics of ET through the protein are not altered in this system. Theoretically, a limiting cathodic current should be observed when the rate of enzymatic proton reduction is slow compared to the rate of interfacial ET from the electrode to the protein. When these conditions are satisfied, the limiting current is directly related to the maximum turnover of the enzyme for the reduction of protons at a given pH. As the CVs indicate, even at the relatively low $[H^+]$ used in our experiments, a limiting current was not observed. This may show that at these currents, a maximum turnover was not reached. There are other explanations for the

observed lack of limiting currents. In one interpretation, a dispersion of nonspecific electrostatic protein-surface interactions (see Figure 1), such as could be the case with our system, preclude the direct observation of a limiting current.[38]

As a complement to the STM images, additional measures were taken to ensure the identity and quantity of *Ca*HydA. To confirm the identity of the protein adsorbed to the surface, SDS-PAGE was run with samples recovered from the Au (111) substrates used for STM imaging experiments against purified *Ca*HydA. Matching bands were observed at 65 kD (Figure 6). The detection of this small amount of protein was also consistent with the STM images in that three samples were combined for the SDS-PAGE, which was just sufficiently above the limit of detection for visualization by silver staining.[55-57] As an independent estimate of amount the *Ca*HydA present on the STM substrate, samples were recovered under denaturing acidic conditions and the Fe was quantified using a modified ferrozine assay.[53,54] Although this assay was near its limit of detection, the amount of Fe observed was also qualitatively consistent with the STM imaging results (Figure 7).

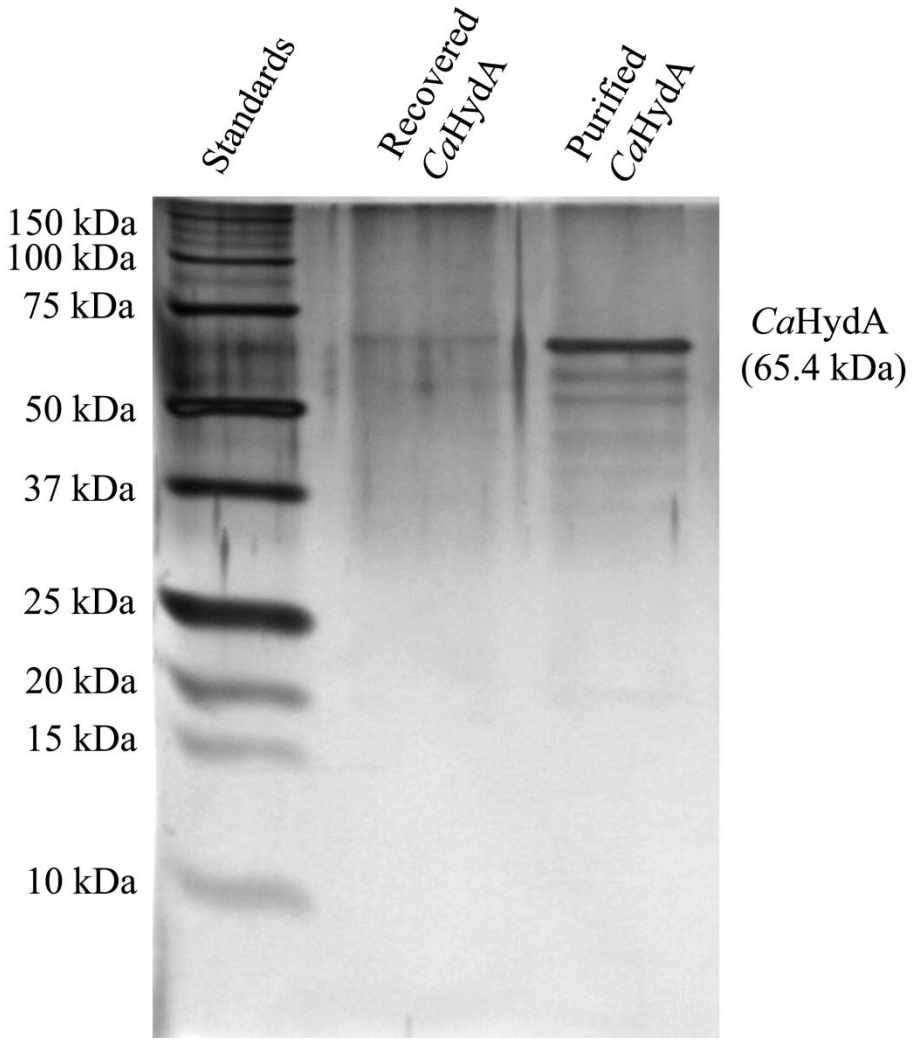

FIGURE 6. Silver stained SDS-PAGE confirming identity of protein recovered from Au (III) surfaces. Left lane: standards. Middle lane: recovered *Ca*HydA from STM substrates. Right lane: purified *Ca*HydA as received.

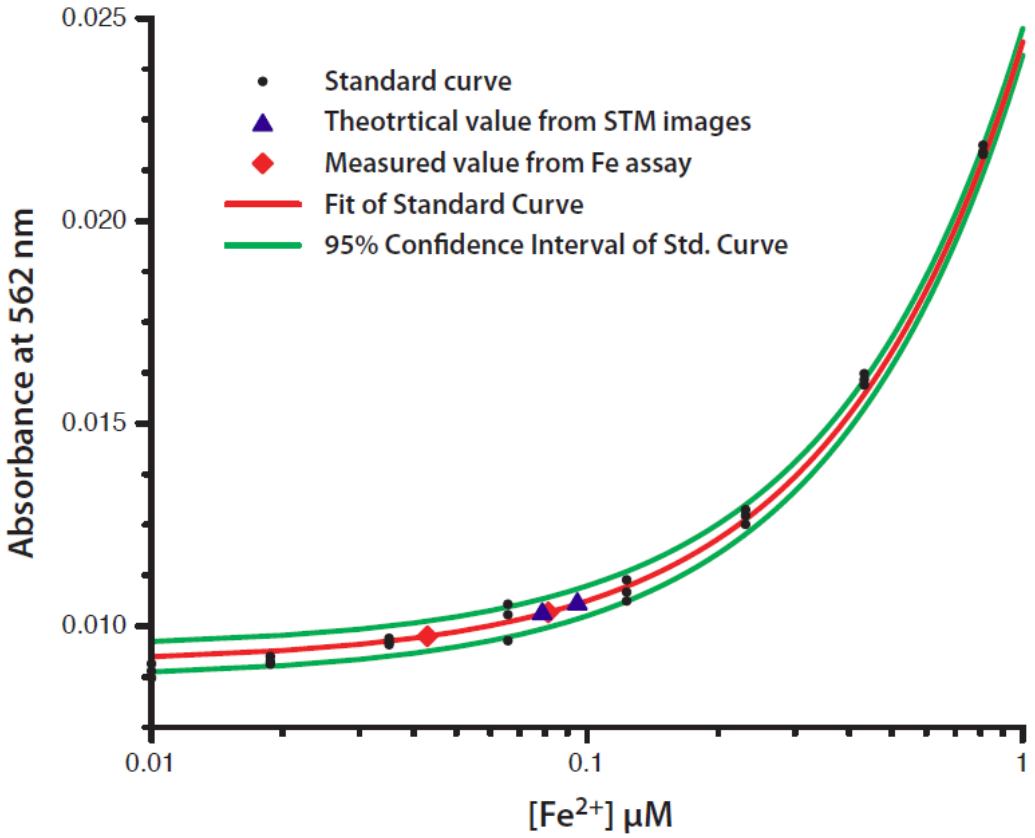

FIGURE 7. Recovered *Ca*HydA ferrozine iron binding assay. Standard curve and recovered samples from STM showing the quantity of iron and corrected to the quantity of protein adsorbed to the modified gold electrodes.

2.5 Conclusion

A method for immobilizing an [FeFe]-hydrogenase, *Ca*HydA, on an atomically flat gold electrode for topographic and electrochemical experiments on catalytically active samples has been described. Direct observation of immobilized protein via EC-STM techniques shows the actual surface coverage which, when coupled with macroscopic electrochemical analysis, allows calculation of TOF as a function of potential at the single molecule level. From our analysis, we observe a TOF of ~1000 s^{-1} for *Ca*HydA on a three carbon SAM, and when extrapolated to bare gold, the TOF is estimated to be ~21,000 s^{-1} at -0.7 V vs. Ag/AgCl. Using a bipotentiostat, resonant tunneling at potentials consistent with the redox midpoints of cofactors within the protein was observed. The β-value of 0.82 $Å^{-1}$ for electron transfer through alkanethiol SAMs measured via determination of catalytic TOF is consistent with values obtained from radically different techniques, such as STM break junction. Taken together, the number of molecules calculated from the images, the exponential fit to the number of carbons in the SAMs, the value of β, and the indication of the redox activity for FeS centers form a consistent picture of electrocatalytic activity of *Ca*HydA on SAMs. However, these results do not fully address the question of heterogeneity in the enzyme's catalytic activity or interaction with the electrode. The stability of immobilized *Ca*HydA on SAMs under these conditions augurs well for future experiments to explore catalytic detail at the single molecule level.

2.6 Future Directions

Eliminating mass transport effects from the experimental setup will help to receive more accurate measurements of turnover. To eliminate mass transport effects, a rotating disc electrode (RDE) setup is commonly employed. With this configuration, an electrode is rotated at rates sufficient eliminate mass transport effects and, thus, diffusion control of a reaction. With hydrogenase modified electrodes, rotation rates of several thousand revolutions per minute (RPMs) are common,[20,26] and, at these rates, *Ca*HydA comes off of the electrode or denatures making it difficult to monitor the catalytic signal. Second, to image the electrode surface with STM techniques requires the use of an atomically flat electrode such as Au (III) or highly oriented pyrolytic graphite (HOPG) which is only conductive through the plane and would be difficult to implement in a RDE setup as special electrical connections must be considered. Also, one must consider the reduction of the Au-S bond if working with SAMs. The electrochemical window that can be utilized for study is limited by the reduction of Au-S bonds that show a large, irreversible reduction current at sufficiently negative potentials. A method to covalently attach the protein to the electrode surface could potentially eliminate many of these problems and allow for a direct measurement of a maximum TOF number, assuming that no other processes limit the reaction, which would allow for direct comparison to other proton reduction catalysts.

2.6.1 Covalent Attachment Methods

Rudiger *et al.* have demonstrated a method for covalently attaching a [NiFe]-hydrogenase to carbon electrode supports using an amide bond between the

surface of the protein and the electrode.[28,36,37] Their method relies on a functionalized carbon surface that bears a terminal amine that can react with carboxylate-terminated residues such as glutamic acid or aspartic acid on the surface of the protein to form a covalent, peptide bond. Functionalization of the carbon electrode takes place via the reductive deposition of a diazonium containing salt. This work utilized a 4-amino-benzenediazonium to produce a positive charge on the electrode surface and was reacted with carboxylates on the surface of the protein to form a peptide bond and a stable protein-electrode interaction resulted for several days. This technique seems promising as a means to attach hydrogenases to electrodes so work was undertaken to covalently bond *Ca*HydA to graphite electrodes for increased stability during electrochemical and imaging experiments.

First, *Ca*HydA was modified with a diazonium salt by a carbodiimide coupling reaction. The protein-diazonium construct was subsequently electrodeposited onto the electrode surface through formation of a C-C bond. Electrodeposition occurs at negative potentials and proceeds via a radical mechanism whereby the diazonium compound loses molecular nitrogen, forming a radical cation that then attacks the electrode surface resulting in a covalent bond.[68] Electrodes prepared in this manner show a characteristic hydrogen production signal and retained activity for at least several hours under working conditions.

Currently, only one diazonium salt has been used for *Ca*HydA couplings, 4-carboxy-benzenediazonium. The carboxylate functional group of this molecule

should react with primary amine residues on the surface of *Ca*HydA forming a covalent amide bond. Similarly, a diazonium salt with different functionality could be synthesized to interact with other residues on the protein surface and possibly alter the orientation on the electrode. The emphasis for this work has been on achieving a stable electrode attachment, and no attempt has been made to specifically orient the protein on the surface.

Using a HOPG electrode, the covalent attachment between the protein and electrode surface can take place resulting in a hydrogen production signal. When cyclic voltammetry is performed on an HOPG electrode with hydrogenase in solution and not covalently linked to the surface, no catalytic hydrogen production signal is observed. This is due the hydrophobic nature of the basal plane of the HOPG electrode. Electrical conductivity to the protein in solution from the electrode surface is not favorable; rather, the electrode is conductive parallel to the surface, or through the plane. Purified hydrogenase is hydrophilic and soluble. For these reasons, it does not interact with the hydrophobic surface and no hydrogen production signal is observed. When a covalent linkage to this surface is made, electrical conductivity is established, thereby creating a method to observe electrochemically driven catalytic hydrogen production. Hydrogen evolution was observed after hydrogenase molecules were decorated with diazonium salts (4-carboxybenzenediazonium) through an amide linkage and the resulting construct is electroreduced onto the surface.

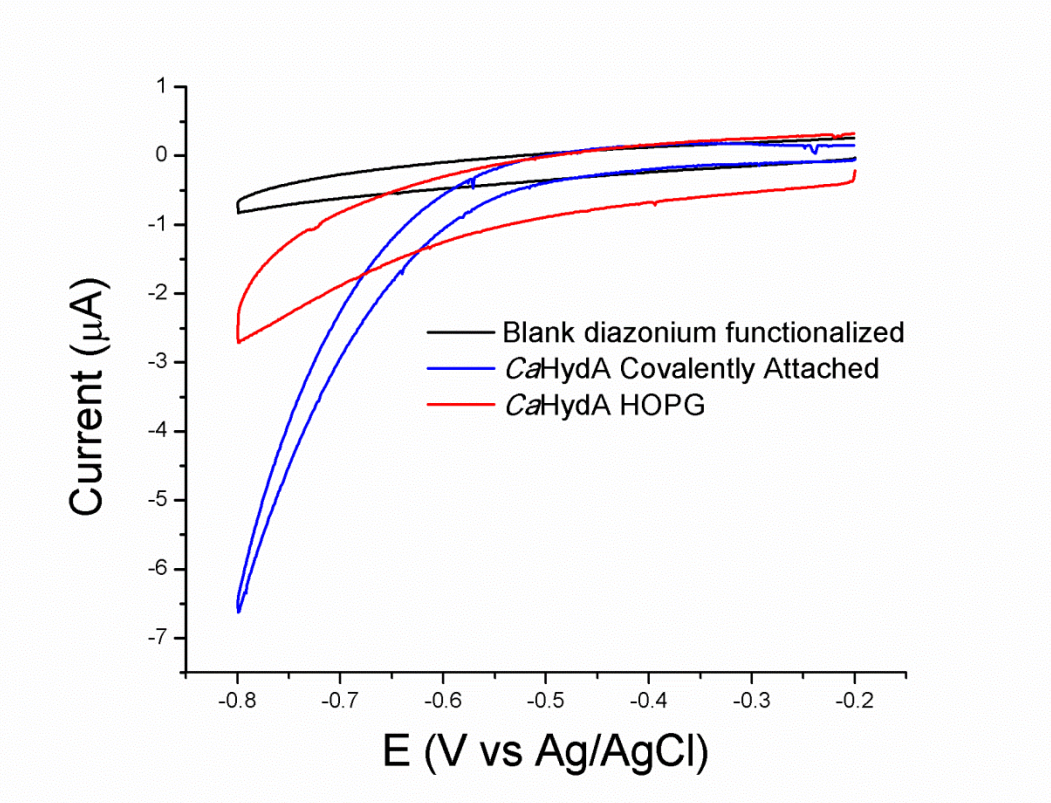

FIGURE 8. Cyclic voltammograms of a HOPG electrode modified with diazonium decorated hydrogenase. Black scan is a blank diazonium functionalized electrode. Red scan is hydrogenase free in solution on the HOPG electrode. Blue scan is bound hydrogenase on the HOPG electrode.

The protein-electrode construct resulting from this attachment chemistry has been investigated as a means of increasing the stability of the system and will enhance future electrochemical STM studies.

2.7 Conclusions and Outlook

To date, the catalytic efficiency of hydrogenases remains an estimate although it is expected to be in the same range as the best proton reduction catalysts, namely platinum. With current techniques and methods, it is possible to observe single protein molecules on an electrode surface and perform macroscopic electrochemical measurements on the same, catalytically active samples. Due to limitations in this experimental setup, i.e. the protein electrode interaction, SAM desorption and lack of mass transport control, better attachment methods are necessary. Initial results with covalent linkages have proven somewhat fruitful although the details of how to orient the protein and obtain high surface coverages have yet to be worked out. Provided that mass transport limitations and protein desorption can be eliminated from the equation, it should be possible to directly measure the maximum TOF of the enzyme. It will also be possible to measure the exchange current of the hydrogenase, which will allow for direct comparison to catalysts such as platinum for proton reduction. A stable and long lasting protein electrode attachment also has applications for technological uses such as fuel cells and larger scale hydrogen production systems where stability and reliability are of great concern. With more work in this area, the maximum turnover of *Ca*HydA will be measured and the limiting factors elucidated. Technological applications may also be realized and implemented into our daily lives.

CHAPTER 3
PHOTOSYNTHESIS

3.1 Introduction

3.1.1 Natural Photosynthesis

Photosynthesis is the process by which organisms utilize photons from sunlight to fix carbon from the atmosphere into a form of stored chemical energy.[69] Globally, photosynthesis converts solar energy into energy dense products such as sugars at a rate of ~133 TW per year,[70] far surpassing current human demands and fueling nearly every aspect of life as we know it. Photosynthetic processes occur in a variety of organisms including cyanobacteria, algae and of course higher plants. While photosynthesis in bacteria and higher plants is related, there are some key differences that must be addressed. First, the pigments, or chromophores, involved in solar energy capture are different; chlorophylls are found in algae and plants whereas bacteriochlorophylls occur in purple photosynthetic bacteria. While both molecules are based on a magnesium porphyrin structure, there are differences in the substituents that in turn lead to a difference in absorption spectra, a difference in the wavelength of light that each can utilize. Bacteriochlorophylls typically absorb from ~670-1040 nm depending on the form, while chlorophylls generally absorb slightly shorter wavelengths. Chlorophyll *a* for example, the core pigment in photosynthetic processes, has absorption maxima at ~430 nm and ~662 nm and is found in organisms that perform oxygenic photosynthesis. Another key difference is in the structure of the light harvesting, or antenna, complexes in the reaction centers of the different

organisms, wherein the chromophore pigments are located and light is absorbed and transferred into a potential. In general, the bacterial reaction center consists of a protein backbone of four separate subunits incorporating two bacteriochloropyll b molecules, two bacteriopheophytin b molecules, two quinones (Q_A and Q_B) and a carotenoid capable of performing light harvesting reactions. The relatively simplistic structure of this complex inherently limits its efficiency as it incorporates a very limited number of chromophores. The photosystem II (PSII) reaction center found in oxygen evolving organisms incorporates six chlorophyll molecules as well as two pheophytin molecules and a pair of plastoquinones. When combined with photosystem I (PSI), the number of antenna pigments jumps to over one hundred, thus vastly increasing the efficiency of photosynthesis.

To fully understand how energy from sunlight is converted into a useable, chemical energy, one must start with chromophore excitation followed by electron flow from H_2O to PSII through PSI to produce the useable energy carrying molecules NADPH and ATP. These processes can be explained by 'Z-scheme' of photosynthesis, which is a way to show the electron transport chain of the whole process.

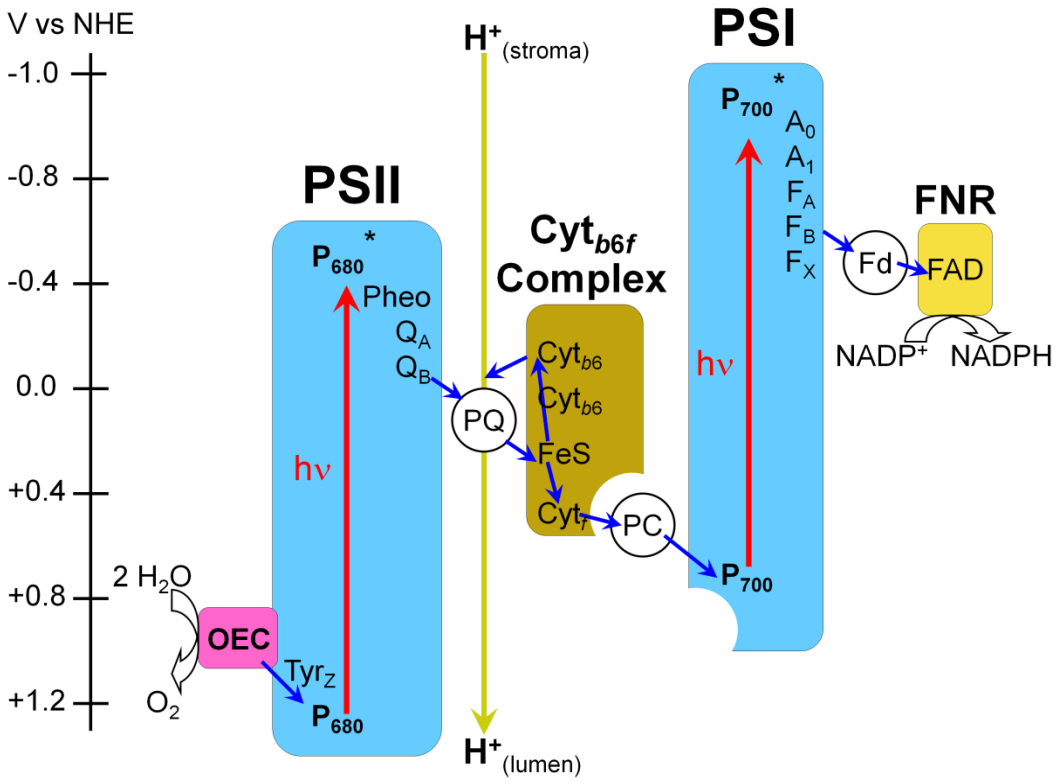

FIGURE 9. The 'Z-scheme' of oxygenic photosynthesis. Photosystems I and II serve to transfer electrons from water to $NADP^+$, thereby creating NADPH while also pumping protons across the thylakoid membrane.

The initial light dependent reactions of photosynthesis occur within the complex transmembrane structure of PSII, which contains a tetranuclear manganese structure known as the oxygen evolving complex (OEC). It is the OEC that oxidizes water to produce protons, molecular oxygen and, most importantly, electrons according to the reaction:

$$2\ H_2O \leftrightarrows 4\ H^+ + O_2 + 4\ e^- \qquad (2)$$

The main reaction center pigment of PSII, P680, is located in close proximity to the OEC and acts as an electron acceptor in its excited state ($P680^+$), thus accumulating positive charge on the OEC upon light absorption. Once four positive charges have accumulated on the OEC, it is capable of releasing four electrons by splitting two molecules of water. From here, electrons flow to cytochrome b_6f via soluble quinone molecules, where the cytochrome *b6f* complex oxidizes quinol and pumps protons across the membrane, creating a proton gradient. Following oxidation of quinol, reduction of plastocyanin takes place which then diffuses to PSI and donates an electron to the primary donor of PSI, $P700^+$. In PSI, light absorption by P700 leads to the reduction of ferredoxin and ultimately the reduction of $NADP^+$ to NADPH while ATP is formed from the resulting proton gradient. These are both reduced products that power the reduction of carbon dioxide (CO_2) to carbohydrates during the dark reactions of photosynthesis, and it is this process which has provided the stored chemical energy that society relies upon in the form of fossil fuels.

3.1.2 Artificial Photosynthesis

The development of human derived technologies for the conversion of solar energy to readily accessible forms of fuel can be broadly referred to as 'artificial photosynthesis.' The sun delivers energy at a rate of ~120,000 TW,[71] orders of magnitude higher than current human demands, making it a very attractive place to look to meet future energy needs. While practical methods for the conversion of solar energy to electricity exist, they currently cannot compete with the cost, abundance and ease of use of fossil fuels. Based on what has been learned from natural photosynthetic systems, artificial systems have been devised resulting in systems that, while expensive, show that it is possible for purely technological systems to produce fuel from sunlight. A fuel is a compound which stores energy in chemical bonds that, when oxidized, releases energy that is capable of being utilized to perform useful work. To create the fuel, a minimum of two things must happen: 1) absorption of sunlight by an antenna pigment forms the excited state of the dye and 2) a reaction center or catalyst that is capable of carrying out charge transfer reactions with the excited dye and can then can perform the desired chemical reaction that ultimately forms the fuel. Progress in both of these fields has allowed researchers to couple pigment and catalyst to form a system capable of utilizing sunlight to produce fuel.

One recent example of a man-made system that can use sunlight to produce a reduced fuel is that of the 'artificial leaf,' concocted by Nocera and coworkers in 2011.[72] Their system utilizes sunlight to produce fuel (H_2) and oxygen directly, showing that humans can, in fact, implement purely

technological designs to produce useable fuels from sunlight. While of interest, systems such as these are not yet competitive with fossil fuels although they do prove the concept. Similarly, the Gust, Moore, Moore group has synthesized organic molecules capable of mimicking the charge separated state in photosynthesis.[73,74] These molecular triad molecules, consisting of a porphyrin core with a carotenoid electron donor and a fullerene (C_{60}) electron acceptor are capable of forming a long-lived (i.e. ns timescale) charge separated state. A long-lived charge separated state is necessary to allow sufficient time for a chemical species to diffuse in and allow for a reaction to take place to produce a fuel, or reduced chemical species.

An excellent example of an artificial system that utilizes a biological component is the photoelectrochemical biofuel cell described by Hambourger and coworkers in 2008.[26] This system uses a porphyrin sensitized photoanode constructed of nanoparticulate titanium dioxide TiO_2 on a conductive glass substrate (fluorine-doped tin(IV) oxide, FTO) for the anodic portion of the fuel cell. Upon porphyrin excitation, electrons are donated from the excited state dye to the conduction band of TiO_2 and enter the circuit of the fuel cell. On the cathodic side of the cell, an [FeFe]-hydrogenase from *Clostridium acetobutylicum*, *Ca*HydA, was used to produce hydrogen from the electrochemical potential generated by the photoanode, thus producing a useable fuel from sunlight. The cell utilizes β-nicotinamide adenine dinucleotide (NADH) in the reduced form as a sacrificial electron donor for the porphyrin sensitizer, which upon donating electrons to the oxidized porphyrin following sensitization

of TiO_2, is oxidized to NAD^+. While a good example of human ingenuity and the technology that exists, a system that is fully sustainable will not utilize a sacrificial electron donor such as NADH. Other limitations exist in this system as well. The extreme oxygen sensitivity of the enzyme inhibits operation except under strictly anaerobic conditions, for example, and the efficiency of the cell would have to be vastly improved to make it viable for large scale hydrogen production.

3.1.3 Natural Photoprotection

It is important to note that under conditions where more incident light is prevalent than a photosynthetic organism can sufficiently utilize, protection mechanisms are in place to protect the organism from photo-damage. These protection mechanisms typically employ ways remove excess electrons that would ultimately end up causing irreparable damage to the organism. One such mechanism employed by plants is nonphotochemical quenching (NPQ) which is triggered by a reduction of pH in the thylakoid lumen under high light conditions.[75] Electron transfer in the reaction centers triggers the pH reduction while also creating a charge gradient across the membrane. The chemical potential stored in this gradient is what powers many of the subsequent reactions of photosynthetic energy conversion. This reduction of pH signals that the electron transfer steps are outpacing the fuel producing reactions that consume the pH gradient for ATP synthesis in the photosynthetic scheme. NPQ converts the excess excitation energy from the antenna complex to heat before damage to the photosynthetic apparatus can occur.[76,77] It is also possible for the excited state of a

chromophore (chlorophyll) molecule to release excess energy by fluorescence, returning it to the ground state and preventing oxidative damage to the organism. In either case, when excess excitation energy is encountered within the photosynthetic apparatus, Nature has mechanisms in place to account for the stress and prevent permanent damage to the organism.

Similarly, excess electrons can be transferred to proteins such as hydrogenases which act as a sink for electrons, combining those electrons with protons to produce molecular hydrogen. Rather than transferring electrons from PSI to $NADP^+$ to produce NADPH, ferredoxin is able to shuttle electrons to hydrogenases for hydrogen production, combining protons from water with electrons from PSI. This is a different photosynthetic protection mechanism for organisms whereby excess electrons can be directed away from the photosynthetic apparatus, thus preventing damage. Photosynthetic hydrogen production typically occurs under conditions of stress, such as low sulfur, whereby electrons are diverted to hydrogenases to allow for continued photosynthetic ATP synthesis, while still preventing damage to the organism. Rather than simply dissipating excess energy as heat as with NPQ, a useable fuel is created making hydrogenases and the process of producing hydrogen simply from sunlight and water of great interest for technological purposes.

3.2 Results

Synthetic molecules that have the ability to regulate their function in response to external stimuli are rare although some have been reported. Recently, the Gust, Moore, Moore group has reported a molecular hexad that functionally mimics the

role of the antenna in NPQ.[78] The molecule features five porphyrin antenna moieties and a pH sensitive dye, comprising a model multichromophoric photosynthetic antenna coupled to a control unit. The core consists of a hexaphenylbenzene moiety to which the five porphyrins and pH sensitive dye are linked. For electrochemical investigations, a model compound was synthesized as seen in Figure 10. Under neutral conditions, the porphyrins rapidly exchange excitation energy and have excited states capable of performing photochemical work. When the solution is made acidic, the dye moiety is converted to an open form that quenches the excited states of all five porphyrins on the picosecond time scale, rendering them kinetically incompetent to carry out additional photochemistry and converting the excitation energy to heat.

There are two possible mechanisms for the quenching of the porphyrin excited states by the open, protonated form of the dye. These are singlet-singlet energy transfer to the dye, yielding an excited state of the dye, and photoinduced electron transfer yielding a charge-separated state. In order to investigate the requirements for quenching by photoinduced electron transfer, the electrochemical properties of the model dye compound were measured using cyclic voltammetry.

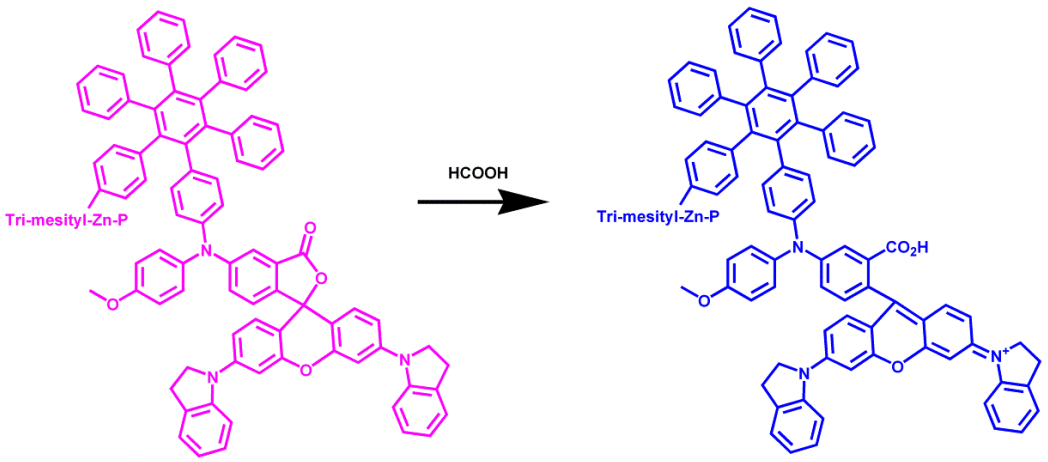

FIGURE 10. Model compound consisting of a hexaphenylbenzene core with one tri-mesityl zinc porphyrin and a pH sensitive dye. Upon addition of acid, the dye goes to its open form, thus quenching fluorescence from the zinc porphyrin.

The results of cyclic voltammetric experiments of the model compound performed in dichloromethane containing 0.1 M tetra-n-butylammonium hexafluorophosphate are shown in Figure 11. Representative results for the model compound containing the dye in the closed, spirocyclic form are also shown in Figure 11 as well as a representative voltammogram after the addition of 20 μL of acetic acid. The first oxidation was observed at 0.94 V vs. SCE, and the first reduction at -1.11 V vs. SCE. Both waves are essentially reversible. The waves around 0.5 V are due to ferrocene, which was used as an internal standard. The addition of acid was necessary to convert most of the dye to the open, protonated form for electrochemical investigation. Although the voltammogram is not reversible, it is clear that reductive processes occur in the -0.5 to -0.6 V region which can be attributed to the dye. The potential for the oxidation of zinc tetramesitylporphyrin (0.68 V vs. SCE[79]) and the reduction behavior of the model dye compound, quenching via photoinduced electron transfer from the excited porphyrin to the protonated dye is thermodynamically possible. However, electron transfer requires overlap of donor and acceptor molecular orbitals, which is expected to be rather weak in the open form of the dye, given the large number of bonds between the porphyrins and dye moiety ortho, meta and para to them and the fact that steric hindrance at the center of the hexaphenylbenzene core leads to near-orthogonal alignment of the central and peripheral benzene rings.

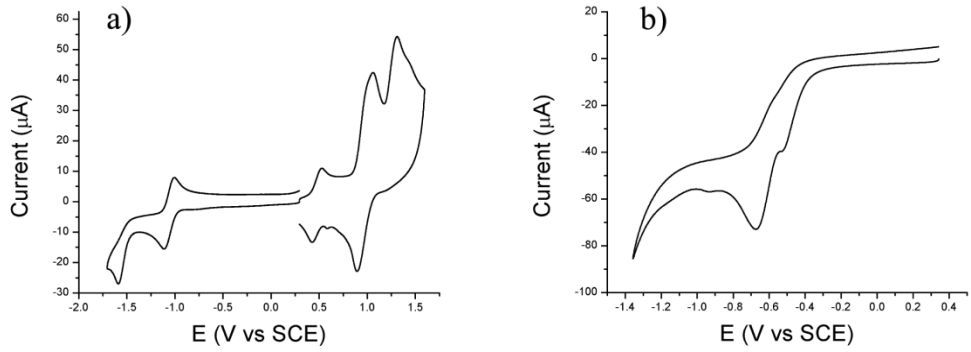

FIGURE 11. Cyclic voltammograms of **a)** model dye compound dissolved in dichloromethane containing 0.1 M tetra-n-butylammonium hexafluorophosphate and **b)** the same solution after addition of sufficient acetic acid to convert most of the dye to the open, protonated form. The potentials were measured with ferrocene as an internal reference and are reported relative to SCE. Ferrocene accounts for the waves around 0.5 V.

3.3 Experimental

Electrochemical measurements were performed with a CH Instruments model 650 C electrochemical workstation. The working electrode was glassy carbon (Bioanalytical Systems, 3.0 mm diameter), the counter electrode was platinum mesh (Alfa Aesar, 99.9 %) and the reference electrode was a silver wire in acetonitrile containing 10 mM silver nitrate with the same 0.1 M tetra-n-butylammonium hexafluorophosphate electrolyte. This reference was used due to its stability under acidic conditions as a titration of acid was necessary to open the dye for these experiments. The potentials were converted to the SCE scale using ferrocene as an internal reference compound.

3.4 Concluding Remarks

This work has shown that it is possible for human designed and engineered systems to be capable of mimicking natural photosynthetic photoprotection processes. The molecular hexad was synthesized in the laboratory, and, when investigated with spectroscopic and electrochemical techniques has been shown to be a synthetic mimic of the natural process of NPQ. When a solution of the model pH sensitive dye compound is acidified by the addition of acetic acid, protonation of the dye converts the closed form to an open form which can then quench the porphyrin first excited singlet state, rendering the complex kinetically incompetent to donate electrons to acceptor moieties under illumination and ultimately converting the excitation energy to heat. Thus, as the acidity of a solution of the model dye compound is increased, the fraction of hexad molecules able to perform useful photochemistry decreases accordingly, and the system

down-regulates its photochemical efficiency. The hexad photochemistry thus mimics the antenna system function in the NPQ photoprotective process in green plants, where antenna chlorophyll excited-state quenching is triggered by a decreasing pH in the thylakoid lumen, and the excess excitation energy is dissipated as heat. In addition to providing a model framework in which to investigate the principles underlying natural NPQ, the molecular hexad shows that incorporation of self-regulation of function in response to external stimuli is also possible in human-made nanosystems for solar energy conversion.

CHAPTER 4

MOLECULAR ELECTRONICS

4.1 Introduction and Background

Interest in utilizing synthetic molecules for electronic devices dates back to the 1970's to work performed by Aviram and Ratner.[80] In the following 40+ years, there has been a drastic increase in interest in studying the electronic properties of single molecules for technological purposes, and a variety of techniques have been developed to do so. Recently it has become possible to measure charge transport and electronic properties of single molecules contacted between two metal electrodes and work in the field is becoming routine practice.[81] However, a thorough understanding of how molecules behave while contacted to two electrodes and how they interact with their environment is still lacking. While a variety of techniques successfully measured single molecule electronic properties, scanning probe techniques, and specifically STM techniques, have been instrumental in the field. Synthetic molecules and biomolecules alike have been studied using these techniques, and much information has been gathered about their electronic properties on the single molecule scale.[82-84] While research in the field is advancing rapidly, there is much research to be done, and the technological implications are endless. Synthetic molecules that act as diodes and transistors have been investigated, and new molecules are being designed to tune the electronic properties to the desired specifications. The work described in the following pages outlines a single-molecule ambipolar field effect transistor (FET) consisting of a perylene core.

A FET is a class of transistor that uses an electric field to control the conductivity of a channel of a semiconducting material, allowing for control of current flow based on an electric field rather than an input voltage. A typical FET consists of a carrier source, a carrier drain and a gate that creates the electric field to drive carrier movement and channel conductivity. FETs are generally classified as n-type, which conduct electrons, or p-type that conduct holes. An ambipolar FET is an electronic device that can be switched between n-type and p-type transport behaviors simply by changing the gate voltage. Unlike its unipolar, n-type or p-type, counterparts whose conduction is dominated by a single type of charge carrier, electrons or holes, the conduction in the ambipolar FET can be switched between either electrons or holes, depending on the gate voltage. Ambipolar transport behavior was first realized with amorphous silicon devices, where both charge carriers are provided by trap states in the material.[85] In more recent years, ambipolar conduction has been reported in several post-silicon devices, including carbon nanotubes, graphene and organic crystals and polymers, and, more recently, in topological insulators.[86-90] However, a single-molecule ambipolar FET has not been demonstrated to date although single-molecule FETs have been investigated. The unique ambipolar function presents new design principles for both analog and digital devices, and new opportunities to study both electron- and hole-dominated transport behavior in the same molecule and to understand the role of the highest occupied molecular orbital (HOMO) and lowest unoccupied molecular orbital (LUMO) in the conduction properties of the molecule.

4.2 Single-molecule Ambipolar Transistor

This work reports a single-molecule ambipolar FET whose conduction behavior can be switched between n- and p-types with an electrochemical gate. To observe an ambipolar effect in a single-molecule junction, molecules with a low HOMO-LUMO energy gap are required.[91] This work describes a pyrrolidine-substituted perylene derivative with a low HOMO-LUMO energy gap that was synthesized and bridged between two gold electrodes, the tip and substrate of an EC-STM setup, using thiolated terminal groups. The Fermi energy levels of the gold electrodes lie within the HOMO-LUMO energy gap of the molecule close to both HOMO and LUMO energy levels. By changing the gate voltage, it is possible to alter the Fermi levels towards the HOMO or LUMO levels, leading to p- or n-type conduction mechanisms depending on the voltage. The results are supported by optical spectroscopy, electrochemical data and density functional theory (DFT) calculations. As a control, an unsubstituted perylene derivative has also been investigated, which exhibits solely n-type behavior, further supporting the ambipolar character of the molecule and the interpretation of the charge transport mechanism in the pyrrolidine-substituted perylene derivative. N-type transport in the substituted molecule is similar to that in the unsubstituted molecule, while the p-type transport in the former derivative is explained by an incoherent multistep tunneling process.

The experimental setup is shown in Figure 12 where a molecule with a perylene core is bridged between two gold electrodes (i.e. the source and drain) to form a molecular junction between an STM tip and Au (III) substrate. The setup

is immersed in an electrolyte, and the charge transport in the molecular junction is controlled with an electrochemical gate electrode immersed in the same electrolyte. This electrochemical gating method is more efficient than the traditional oxide gate in conventional semiconductor devices,[90,92] and has been used previously to demonstrate FET behavior in single-molecule junctions.

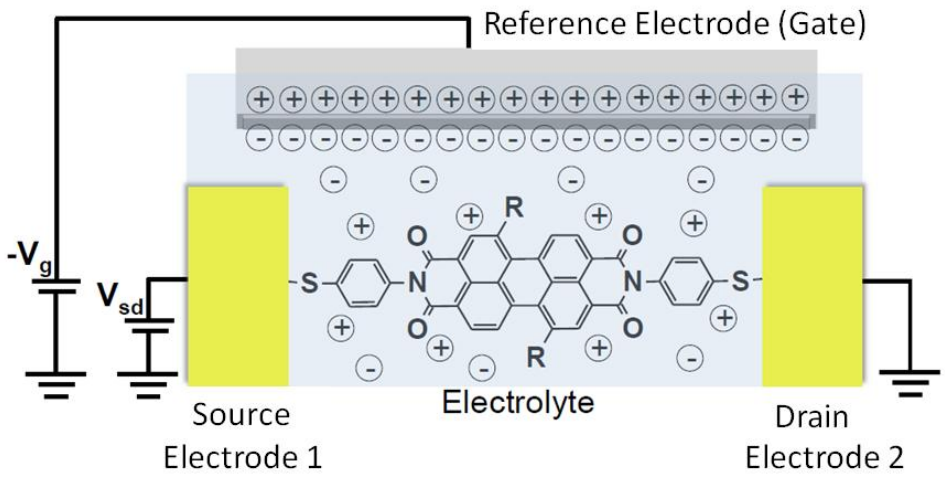

FIGURE 12. Schematic of the experimental setup of single-molecule FETs measured in this work. Source (electrode 1) and drain (electrode 2) are the Au surface and the tip electrodes respectively in the employed STM configuration.

Two molecules were used for this study, a 1,7-dipyrrolidine-substituted 3,4,9,10-perylenetetracarboxylic diimide (PTCDI) and an unsubstituted PTCDI. The latter serves as a control molecule which shows only n-type conduction behavior. All synthetic work required for this study was performed by collaborators at the University of Utah, and molecules were used as received without further purification. Both molecules contain two terminal mercaptophenyl groups at the N-imide positions on both sides of the molecule that serve to both covalently anchor (through thiol-gold bonds) and electronically couple the molecules and the two gold electrodes.

4.3 Experimental Techniques and Measurements

The absorption spectra of the two molecules used for this study show that the pyrrolidine substitution to the PTCDI backbone causes a red shift in the absorption spectrum (Figure 13), which indicates a smaller HOMO-LUMO energy gap than the unsubstituted molecule. This observation is consistent with previously reported works of redox-active chromophores with pyrrolidine substitutions.[93] The optical absorption data provide useful information about the HOMO-LUMO energy separation, but it does not tell give information about the alignment of the HOMO and LUMO energy levels of the molecule relative to the Fermi energy levels of the gold electrodes. To access this information, electrochemical measurements of the molecules adsorbed on gold electrodes and in solution were performed. Due to the relative low coverage of the molecules on the gold surfaces, differential pulse voltammetry (DPV) was used for experiments on adsorbed species. DPV suppresses background polarization current and helps

to resolve the peaks in the voltammogram due to molecular redox processes. As shown in Figure 13, the anodic (HOMO-related) redox peak of the pyrrolidine-substituted PTCDI experiences a cathodic shift of ~0.6 V relative to that of the unsubstituted PTCDI molecule. This observation indicates that the pyrrolidine substitution not only reduces the HOMO-LUMO energy gap separation, but also results in a closer alignment of the HOMO energy level to the gold electrode Fermi energy.

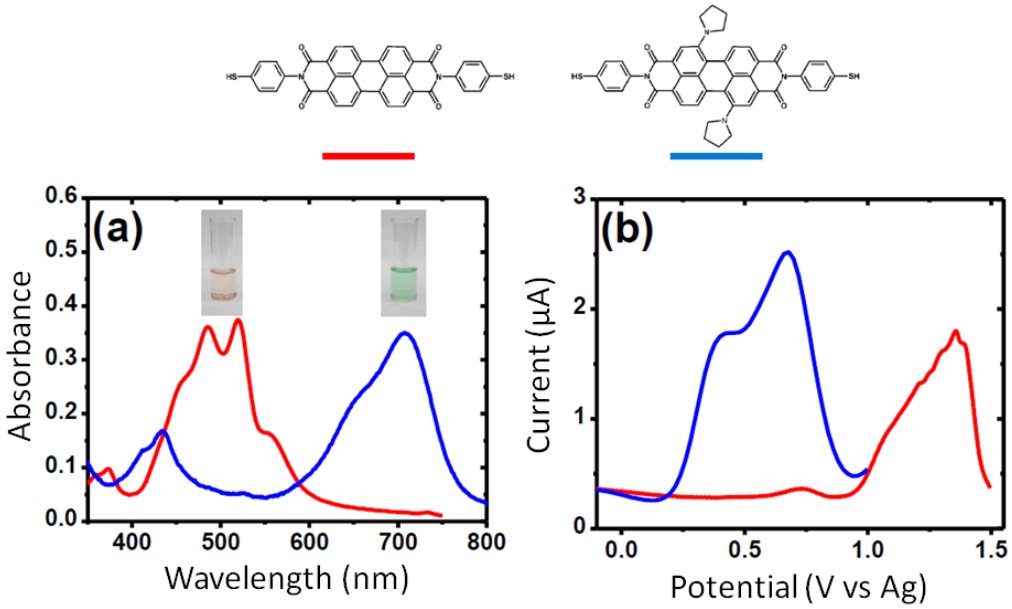

FIGURE 13. UV-visible absorption spectra **a)** and differential pulse voltammograms (DPV) of Au (111) surface modified with molecules and **b)** for the unsubstituted PTCDI (red lines) and the pyrrolidine-substituted PTCDI (blue lines). All measurements were performed in acetonitrile with 20 mM tetrabutylammonium hexafluorophosphate ($TBAPF_6$) as the supporting electrolyte. The inset in **a)** shows photos of acetonitrile solutions of the two molecules. The electrochemical pulse parameters in **b)** were 0.5 s interval time and 30 mV amplitude.

For comparison, electrochemical measurements on the pyrrolidine-substituted and unsubstituted PTCDIs dissolved in the electrolyte rather than adsorbed on the electrode surfaces (Figure 14) were also performed. Although the cathodic (LUMO-related) processes are barely resolved for the unsubstituted PTCDI, most likely due to the extremely low solubility of the molecule, the relative shift in the anodic (HOMO) peak between the two molecules is consistent with the measurements on adsorbed molecules shown in Figure 12.

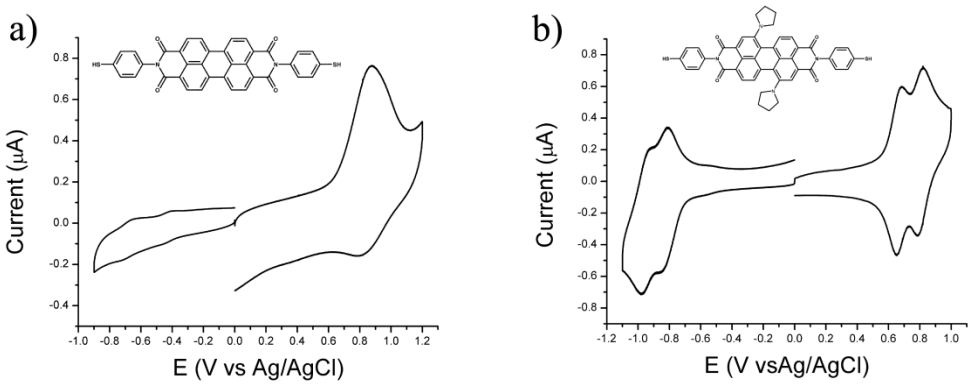

FIGURE 14. Cyclic voltammetry on polycrystalline Au electrodes for the PTCDI molecules dissolved in benzonitrile with 20 mM $TBAPF_6$. **a)** unsubstituted PTCDI and **b)** pyrrolidine-substituted PTCDI. $\nu = 50$ mV/s.

After the characterization of the energy levels alignment between both molecules and the gold electrodes, charge transport in single-molecule junctions of the pyrrolidine-substituted and unsubstituted PTCDI molecules was measured using a scanning tunneling microscope (STM) break junction method adapted from previously reported procedures. Briefly, an Apiezon-coated Au STM tip was brought into contact with a gold substrate electrode covered with a layer of the target molecule, during which the current flow between the tip and substrate electrodes under a fixed applied bias voltage (V_{bias}) was monitored continuously. When the current reached a preset value, the STM tip was retracted until the current dropped to a lower current set point. The process was then repeated, and a large number of current traces were recorded during the retraction stage. Figure 15 plots some individual conductance traces for the pyrrolidine-substituted and unsubstituted PTCDI molecules. Each trace in the figure displays a step-like feature, which is attributed to the formation of a single molecule junction. Approximately 40% of all recorded individual traces show such step-like features. Within the traces that contain the step-like feature, about half show rather flat steps while the other half clearly show tilted step features. The titled steps have been observed in other single-molecule junctions containing rigid conjugated backbone, such as the perylene used in this study, and they have been attributed to overlapping between the pi-orbitals of the conjugated molecular block and the orbitals of the two metal electrodes. This orbital coupling contributes to a larger conductance for these molecules, but it decreases as the distance between the two electrodes is increased by pulling them apart, leading to a gradual decrease in the

conductance, which is observed as a tilted step in the conductance vs. distance trace (red curves in Figure 15a). In contrast, the traces with flat steps correspond to the molecular configurations in which the coupling of the pi-orbitals with the electrodes is minimal (*e.g.* the molecule in the last stage of pulling is perpendicular to the electrode surface). In this case, the conductance values correspond almost exclusively to the conductance through the molecular backbone. To avoid ambiguity in determining the conductance of the molecules, conductance histograms were constructed by including traces showing flat steps only (black curves in Figures 15 a) and b)). Figures 15 c) and d) are the conductance histograms for the unsubstituted and pyrrolidine-substituted PTCDI molecules, respectively, each showing a distinct peak marked by an arrow. The blue lines in the figures are gaussian fits to the peaks, from which conductance values for both unsubstituted and substituted molecules are determined to be 8.8 x 10^{-6} G_0 and 4.5 x 10^{-5} G_0, respectively (G_0 = 77.4 μS is the conductance quantum). Control experiments were carried out by following analogous sample preparation procedures in the absence of the target molecules. The measured conductance traces do not display any step-like features, and consequently the conductance histogram shows no peak.

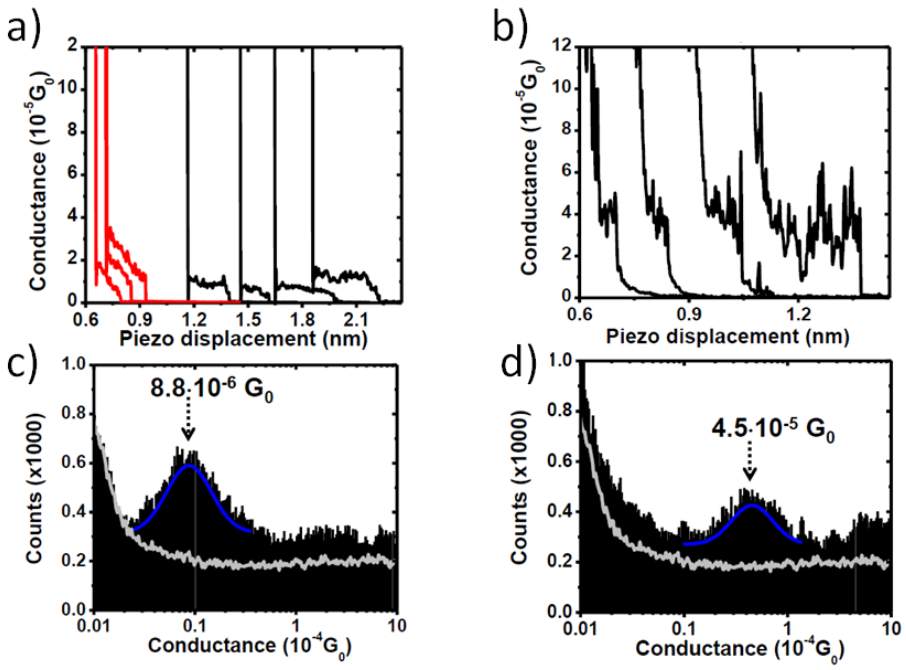

FIGURE 15. Single-molecule conductance experiments. **a)-b)** are representative pulling traces for the unsubstituted and the pyrrolidine-substituted PTCDI respectively. Red curves in **a)** are typical pulling traces displaying lateral coupling effects. **c)-d)** Conductance histograms built from thousands of the black traces in **a)** and **b)**. The single-molecule conductance values are taken from the gaussian fits (shown as blue lines) of the most prominent peaks in the histograms. The grey lines are the conductance histogram in the absence of molecules. The electrochemical gate voltage for the W1 electrode was set to 50 mV and the sample V_{bias} to 0.2V.

To study the electrochemical gate effect with both molecules in the junction of the STM setup, the "blinking" method was used as described previously in the literature.[82,94,95] With this method, the Au STM tip electrode was brought close to the substrate electrode on which the sample molecules were adsorbed via Au-thiol bonds. The separation between the tip and substrate was controlled by the STM feedback loop to the current, which was initially set to a value less than 20 pA, with a corresponding tip-substrate separation of ~2 nm, slightly smaller than the PTCDI molecular length (~2.3 nm from S to S). The feedback loop was then switched off and the current was monitored continuously. Once a molecule forms a bridge between the Au (III) surface and the tip electrodes, a large and sudden increase in the junction conductance was observed and an electrochemical gate voltage ramp was triggered to measure the current through the molecule as a function of the applied gate voltage. Figures 16 a) and b) are some of the current vs. time traces recorded with the "blinking" method, showing sudden, drastic increases in the current from the low initial set-point current to a higher value. The stepwise current increase is due to the formation of a single-molecule bridge between the tip and substrate electrodes, and the conductance determined from the current step agrees well with the conductance value obtained from the conductance histograms shown in Figure 15. Single molecule junctions that lasted for seconds were commonly observed, allowing for the determination of the charge transport behavior through the molecules by sweeping the electrochemical gate voltage. Figures 16 c) and d) show several representative curves of the gate dependent source-drain current for the

unsubstituted and pyrrolidine-substituted PTCDIs, respectively. There is a clear junction-to-junction variation in the gate-controlled current, most likely due to structural differences and contact geometry differences. However, the overall current vs. gate voltage curves show distinct, reproducible trends for both molecules as observed in the average current vs. electrochemical gate characteristics (Figures 16 e) and f)).

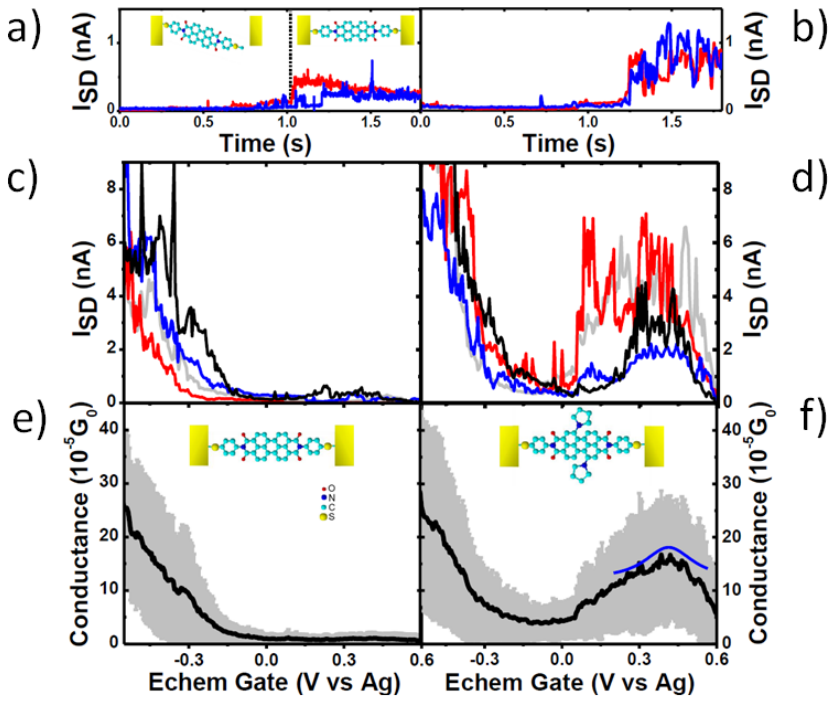

FIGURE 16. Single-molecule FET experiments. **a)-b)** "blinking" traces showing single-molecule bridging events for the unsubstituted and the pyrrolidine-substituted PTCDI. Sudden jumps in the DC current mean formation of a single-molecule junction (see inset in **a)**). **c)-d)** Representative source-drain current vs. electrochemical gate voltage curves of different junctions for the unsubstituted and the pyrrolidine-substituted PTCDI respectively. Different colors in **a)-d)** represents independent measurements. **e)-f)** Average conductance vs. electrochemical gate voltage for the unsubstituted and the pyrrolidine-substituted PTCDI respectively. The grey shadow corresponds to the standard deviation for N=75 and 85 in **e)** and **f)** respectively. The 2-step tunneling model is included in **f)** with a positive Y-offset for a better visualization (blue curve) In all experiments, a constant sample V_{bias} of 0.3V was applied.

The gate voltage range was kept within ± 0.6 V because the single molecule junctions become increasingly unstable outside of this voltage range, causing the breakdown of the junction, which was observed as a sudden decrease in the current to a lower value. For control purposes, electrochemical gate dependence measurements were also performed with the broken junctions within the same gate voltage range. The results show little electrochemical gate dependence, which further validates that the observed gate voltage dependence is due to gate-dependent transport within the PTCDI molecule.

Single-molecule junctions of unsubstituted PTCDI molecules show clear n-type FET behavior, in which the current increases as the gate voltage sweeps negative relative to the reference (electrochemical gate) electrode. This corresponds to the approach of the LUMO to the Fermi levels of the electrodes, leading to an electron-dominated charge transport through the single-molecule junction (Figure 16 e)). This observation agrees well with previous work performed on a similar molecular block carried out in an aqueous electrolyte within a narrower gate voltage range.[96,97] For the pyrrolidine-substituted PTCDI, the gate dependence in the negative voltages shows a clear n-type FET behavior, which is nearly identical to that of the unsubstituted molecule (Figure 16 f)), indicating that the substituted and unsubstituted molecules share the same n-type conduction mechanism at negative potentials. However, the positive gate voltage sweep also leads to an increase in the current through the pyrrolidine-substituted PTCDI molecule, in sharp contrast to the behavior of the unsubstituted PTCDI. Because sweeping the gate positively corresponds to the alignment of the PTCDI

HOMO to the electrodes Fermi energy levels, the increase in the current with positive sweep of the gate voltage indicates a hole-dominated transport, or a p-type conduction mechanism. The results show that the pyrrolidine-substituted PTCDI junctions can be switched from an electron-dominated to hole-dominated transport, thus demonstrating that the ambipolar FET behavior can be achieved in a single-molecule junction by tuning the electronic properties of a molecule by changing substituents to either electron donating or electron withdrawing groups.

Further increasing the electrochemical gate voltage in the positive direction results in a decrease in the current leading to a broad peak centered at ~ 0.5 V, close to the redox peak position observed in the DPV voltammogram (Figure 13 b)). The presence of a peak in the current vs. electrochemical gate curve and the location of the peak near the redox potential strongly suggest a two-step incoherent transport within the pyrrolidine-substituted PTCDI, in which holes tunnel into the molecule from one electrode, and then tunnel from the molecule to the second electrode after the molecular structure and surrounding solvent relax to accommodate the newly oxidized state. Such a two-step charge transport process has been predicted by Kutentzov and Ulstrup,[98] and has been observed in other redox molecules at the single-molecule level.[66]

4.4 Summary and Outlook

In summary, this system demonstrates ambipolar FET behavior in a single-molecule junction by studying charge transport in two structurally related molecules: an unsubstituted PTCDI block and a pyrrolidine-substituted PTCDI block. Optical absorption spectroscopy and electrochemical measurements show

that the introduction of the pyrrolidine groups to the conjugated PTCDI backbone results in a decrease of the molecular HOMO-LUMO energy gap, resulting in a shift of the HOMO level closer to the Fermi energy levels of the electrodes. Using an electrochemical voltage gating method, it is possible to bring either the LUMO or HOMO of the pyrrolidine-substituted PTCDI molecule close to the Fermi energy levels of the electrodes, and to switch the charge transport behavior from electron-dominated to hole-dominated. Furthermore, a peak is observed in the p-type regime of the ambipolar FET, which is attributed to a two-step incoherent transport process. Molecules that exhibit electronic properties such as transistor-like behavior or diode-like behavior will prove vastly influential to the development of new technologies. The ability to easily tune the electronic properties of such molecules also lends them to be studied for technological purposes where a variety of properties are desirable. Characterization of such compounds at the single molecule level bodes well for the future development of devices that are based on synthetic organic compounds.

CHAPTER 5

LAB EQUIPMENT DESIGNS AND CONSIDERATIONS

5.1 Introduction

Due to the nature of working with hydrogenase and performing experiments under strictly anaerobic conditions, much of the work performed in this dissertation utilized equipment that was fashioned in the laboratory or modified from existing equipment. All of the electrodes used for STM and electrochemical investigations were constructed in the lab as well as an entire setup to perform STM under anaerobic conditions. Electrical connections also had to be fabricated to pass through an airtight structure without leakage for a variety of experiments, most notably electrochemical experiments where the electrochemical cell was located inside the anaerobic chamber and the potentiostat was kept outside. The cell used for STM was also modified to incorporate a platinum counter electrode into the design and use a Ag/AgCl reference electrode as opposed to a silver wire pseudo reference. A photo of this cell can be seen in Figure 17.

FIGURE 17. Photo of the EC-STM cell employed for these experiments. Counter electrode is woven into the Teflon® cell and with an electrical connection on the left. A Ag/AgCl reference electrode is on the right and the working electrode is the Au (III) substrate in the center.

5.2 Preparation of PGE Electrodes

Preparation of PGE electrodes was performed by sealing a 3/16" PGE (MinTEQ International, Inc. (Easton, PA, USA)) rod into a Teflon® sheath with a non-conductive epoxy to seal the graphite in the sheath and prevent solution from coming into contact with any face of the electrode except for the desired edge plane. Electrical contact was established through a brass rod contacting the graphite with a conductive, silver-based epoxy. Final resistances for PGE electrodes were <10 Ω per electrode as established with a handheld multimeter and were not changed by polishing the electrodes. Final electrodes were sanded to a smooth surface by gradually increasing the grit of the sanding material from 120 grit to 2500 grit, followed by polishing with various diamond pastes down to 1 μm. Finally, a mirror finish was achieved by polishing in a figure eight pattern with a 0.5 μm alumina slurry. Electrodes were then rinsed and sonicated in Nanopure 18 MΩ cm water to remove excess alumina. The resulting electrode surface was suitable for electrochemical studies and protein adsorption without further modification. Similarly, 2 mm diameter PGE electrodes were constructed with material from GE Advanced Ceramics, which is no longer in business. These electrodes performed very nicely as well for electrochemical investigations although the larger surface area electrodes were used for the majority of the work presented in this dissertation.

5.3 Substrate Preparation

STM techniques require the use of atomically flat electrodes or substrates for imaging and their preparation is quite involved when prepared in the laboratory.

Gold III (Au III) substrates are prepared by evaporating Au onto mica under ultra high vacuum and annealing to ensure formation of the III crystal structure. The following procedure outlines, in detail, how to prepare suitable STM substrates.

1. Before entering the Dr. Tao's clean room in the basement of the Biodesign building, put on gloves, a hair net, shoe covers and lab coat.

2. Cut between 25-30 pieces of new mica of about 1x1.5 cm^2. As a rule of thumb, split the original rectangular mica slice into two parts lengthwise and cut each one into 5-6 pieces. To protect the mica and get clean cut edges, cover the mica slices with a transparency sheet and use the paper cutter in the clean room. Place a sheet of cleaning towel wipe (special for vacuum applications) on the right side of the paper cutter in order to catch the cut mica samples. All these things can be found on the sink in the clean room next to the evaporator.

3. Use "white scotch" tape to cleave both sides of the mica samples and use tweezers carefully cleaned with alcohol to move them into a clean Petri dish for storage. Be sure that you have completely peeled off both mica faces. Place the mica slide with the better peel face up in the Petri dish so that this side will have the gold deposited onto it. In order to preserve similar thicknesses, don't repeat the pealing process more than 3 times.

4. Take the sample holder out of the vacuum chamber and place it upside down over the cylindrical jar available in the bio-hood. Never leave the evaporation chamber open; always use the red-plastic cover with

aluminum foil to seal it to prevent debris from contaminating the chamber (this is also available with the jar).

5. Take an Au pellet from the security chamber (black box located at Microscopy Lab, STM Lab in Biodesign room AL1-15), and sonicate it for 10 minutes in a new plastic beaker with acetone and then 10 min. with isopropanol.

6. In the meantime, position the mica slices onto the sample holder for the vacuum chamber. Start positioning from the first row by releasing the holding metallic bar from the open side only using an Allen wrench. Repeat the process until all rows are filled by mica samples. Tighten metallic bars back down again and check that all mica samples are tightly attached to the holder by turning sample holder back to its original orientation.

7. Dry the sonicated Au sphere with N_2 and place in the Au vaporizer (in the evaporation chamber) by using the "joint-like" conical paper also available next to the sink in the clean room. After placing the pellet in the chamber, align the shutter so that it directly covers the Au pellet.

8. Clean a new copper gasket with the vacuum cloth and isopropanol and use the special pliers labeled "pliers for Cu" to exchange the copper ring that stands on top of the vacuum chamber with the new one. ***Warning***: If the special pliers are not used to remove the old copper ring, scratches can form, which make it harder to pull good vacuum and can permanently

damage the high vacuum chamber. New copper rings are available at the bookcase to the left of the Evaporator in the clean room.

9. Check the deposition sensor microbalance to ensure that it reads over 6.94. If it does not, remove the sensor from the back of the chamber and exchange it with a new crystal. Also repeat step 8 to exchange the smaller copper ring when placing a new sensor within the chamber.

10. Place the sample holder with the secured mica pieces back into the Evaporator. Rotate it until both (up and down) marks match and attach all nuts and bolts tightly. Use washers on both sides of the screws. Try to tighten all screws in the same way in a crosswise pattern to prevent distortion of the sample chamber.

11. On top of the sample holder there are four electrical terminals: 2 for the thermocouple (yellow) and 2 for the heater (red). Plug in the thermocouple ensuring that the Cu and Al leads are aligned correctly. Then attach the Cu substrate heating wires made of tungsten and tighten the Allen screws. Use a multimeter to check that the substrate heating wires are connected to the terminals properly. Then place scotch tape between the wires to prevent a short circuit from occurring during heating and deposition. Additionally, use the multimeter to check that there is not contact between the chamber heating wire and the stand that holds the chamber. If there is, find the short and fix it.

12. Turn on the sink to allow water to flow to the intercool pumps. Ensure a vigorous water flow but not so high as to compromise the clamps holding the hoses onto the cooling pumps.

13. Turn on the power cords for the pumps and vacuum monitoring equipment on both sides of the rack and turn on the mechanical vacuum pump.

14. After 10 minutes of pulling vacuum on the chamber, turn on the turbo pump by pressing "start" in the front panel (Turbotronik).

15. Once the chamber pressure has reached 10^{-6} torr or lower, cover the chamber completely with aluminum foil and turn on the chamber heating system by plugging the right white power chord into one of the Variacs underneath the chamber. Increase the voltage slowly until it reaches around 60 V.

16. After 1 hour, the temperature will be around 55 °C. Then, turn on the substrate heating stage by plugging the second Variac into the sample heating power supply. Increase the voltage slowly up to 80 V. Control the voltage to stabilize the temperature inside the chamber to 360 °C. Once the temperature has stabilized, check that the pressure is at 10^{-7} torr or below (it takes a while to get a stable reading of the pressure). If the pressure is too high, the tungsten wires can oxidize and get brittle and destroy the heating mechanism.

17. Let stand for 20 hours under vacuum and at 360 °C.

18. Turn off the heating system of the chamber (Variac 1, always decrease voltage slowly), and remove the aluminum foil from the heating chamber.

19. After one hour, turn on the degassing device (heating element) to clean the vacuum gauge (~10 min.) and ensure that the pressure inside the chamber is around $5x10^{-8}$ torr.

20. Connect the large wires (red) on the left side to the available Variac.

21. Turn on the quartz crystal microbalance thickness monitor. Hit stop so that it stops reading "fail" and then press start to start the monitor.

22. Release the shutter for the gold heating element. One can confirm that the shutter has been fully released by using the light of the filament to see the shutter.

23. Increase slowly the Variac voltage while monitoring the gold deposition rate until it reaches 1.3 angstroms/second (should be at around 30 V). Note: that the temperature will rise up a little to about 370 °C during the evaporation due to the increased heat of the gold heating stage.

24. Keep this rate until the thickness reaches ~1300 angstroms and then stop the evaporation using the controllable cover in front of the chamber. Turn the Variac off.

25. Let Au/mica samples anneal in the chamber at 360 degrees for 3 hours. This step is imperative as a shorter time does not allow for complete

formation of the Au (III) surface and a longer time can destroy the Au (III) structure and render the samples useless for STM studies.

26. Clean 25-30 glass storage vials in Piranha solution (a 3:1 mixture of concentrated H_2SO_4 and 30% hydrogen peroxide) and rinse a minimum of three times with nanopure water to ensure cleanliness. Dry in the oven <100 °C so that they are ready to use when the substrates are finished.

27. Turn off substrate heating and wait for the temperature to drop to 60 degrees (this will take a couple of hours).

28. Turn off the turbo pump and wait for about 10 minutes. When you can't hear the high-pitched noise from the turbo pump, turn off the mechanical pump and intercooling water and wait for the chamber to reach room pressure (this happens within a few short minutes). This occurs spontaneously as air will leak through the mechanical pump to fill the chamber.

29. Slowly begin to unscrew the nuts and bolts for the substrate holder. If you hear air leaking into the chamber when unscrewing them, retighten and wait for more air to enter through the mechanical pump as to not disturb the samples or cause damage to the Evaporator.

30. Remove the sample holder from the chamber and close the chamber with the red plastic cover.

31. Carefully remove Au/mica substrates and store each one in a clean glass vial from step 26 and seal them with aluminum foil.

32. When finished, replace the red plastic cover with the substrate holder and turn off all power cords.

33. Store all samples in an aluminum foil boat with the deposition date labeled on the side. Place the entire boat in the vacuum chamber in the clean room to prevent contamination. Remember to depressurize and repressurize the chamber slowly so that the substrates do not get knocked over.

The resulting samples are ready to be flame annealed with a hydrogen flame and used in the STM. Gold will be roughly 160 nm thick, so extra care must be taken when working with these delicate samples. Place two microscope slides onto the foil covered brick found in the clean room and arrange in such a manner as to leave a gap slightly smaller than the size of one of the Au (III) substrates created above. Place the substrate to be flame annealed across the gap in the microscope slides being careful not to touch the gold surface. Handling samples with only clean forceps helps to prevent contamination. To anneal, light the hydrogen flame and turn out most of the lights in the room in order to be able to see it. The use of a quartz pipette for the hydrogen flame has proven to be a cleaner and more reproducible method to flame the surface. Hold the flame about an inch from the surface and move rapidly in a circular motion so that the flame covers the Au (III) substrate, taking care as to not burn the surface. If this happens, there will be an

obvious change to the surface and it will appear rough and not shiny anymore. The substrate is now useless and must be discarded. A properly flamed sample will retain its shine and must be used immediately otherwise organic compounds from the air in the lab will cover the surface and show up during STM experiments.

In addition to the lab equipment that was fabricated to perform these experiments, care was also taken to isolate vibrations for STM experiments and to eliminate or mitigate electrical noise. Care should also be taken to eliminate air currents caused by the catalyst fan boxes inside the anaerobic chamber as the mechanical disturbances can cause vibrations and interrupt STM experiments. The atmosphere of the anaerobic chambers is also conducive to corrosion of metals and electrical connections so routing maintenance is necessary. This chapter will describe, in detail, the design considerations, construction and maintenance of much of the lab equipment used for the experiments performed for this dissertation.

5.4 Anaerobic STM Design

Due to the extreme oxygen sensitivity of *Ca*HydA, STM experiments involving protein had to be performed under anaerobic conditions. To do this, a Coy Laboratory products vinyl anaerobic chamber (Model A) was purchased which was large enough to house a stabilization mechanism for the STM. Stabilizing the STM during experiments is essential to eliminate vibrations caused by the building as well as the surrounding atmosphere. Typically, active vibration dampening systems would be used, although due to their price they were not

utilized for these studies. Another vibration dampening mechanism involves suspending the entire STM head from a structure. This was accomplished inside the anaerobic chamber by constructing a scaffold that was 39" high and 24" across in either direction. The scaffold was built out of angle iron and bolted together for a stable structure that was capable of holding many pounds. It should be noted that this structure was far too large to be entered into the anaerobic chamber when completed, so construction had to take place entirely inside the anaerobic chamber. Once completed, bungee cords were attached to the structure from which a modified concrete block weighing ~10 pounds was suspended. An additional 5 pound weight was placed on top of the block to increase the weight suspended from the structure. The weights oscillate from the structure at a frequency of ~1 Hz, which dampens most of the frequencies that would cause interference with the STM. To further dampen vibrations and isolate the STM from the ground, the entire glovebox was placed on eight racquet balls, which have been quite useful for many years for STM isolation in Dr. Tao's lab. Together with the STM hanging from the structure inside the anaerobic chamber, the STM was stable enough for high resolution imaging under strictly anaerobic conditions.

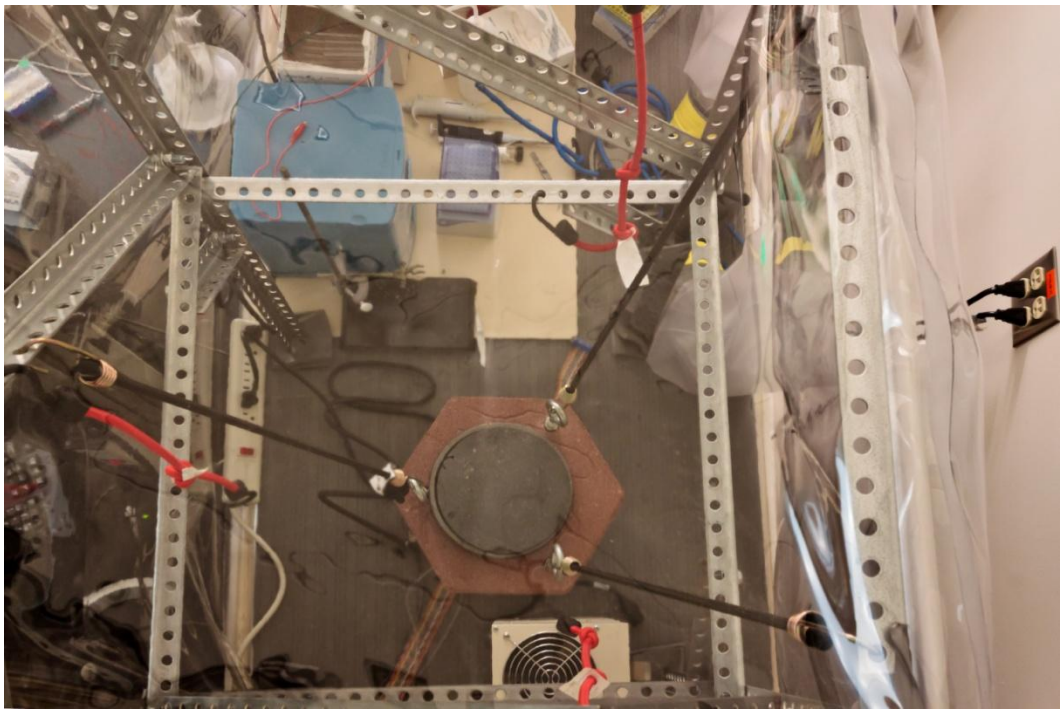

FIGURE 18. Photo of the STM vibration isolation mechanism constructed within the anaerobic chamber.

Another consideration of working in the anaerobic chamber is that the palladium catalyst boxes incorporate fans that cause a mechanical disturbance inside the chamber. There are a variety of ways to combat this but the simplest is to turn the fans off briefly while performing imaging experiments. However, the fans can only be off for ~30 minutes before oxygen levels rise to the point where they can inhibit the enzyme. Another option is to cover the STM with a piece of foam, designed for just this purpose, which keeps the turbulence from the fans from disturbing the STM. While this option works well, maneuvering in the anaerobic chamber can be challenging and the cover is large, making it difficult to put in place and remove. For the work performed with hydrogenase one or both of the options discussed above was used.

5.5 Electrochemical Considerations

In addition to the STM experiments, electrochemical experiments also require special attention when performed in the anaerobic chamber as the electrical connections must go through the chamber without leaking. This was accomplished by placing conductive brass rods through a rubber stopper and sealing them into place with silicone sealant. The rubber stopper was then inserted into an opening in the glovebox and again sealed in place with silicone sealant. Electrical leads from the potentiostat were than attached to the brass rod on the outside of the glovebox and corresponding electrical connections were made inside the glovebox for electrochemical experiments. Both anaerobic chambers employed for these studies used analogous electrical connections and they performed without fail for the duration of these experiments. It should be noted

that the connections will need to be cleaned with sandpaper occasionally to remove corrosion and ensure good electrical contact on both the inside and outside of the anaerobic chamber.

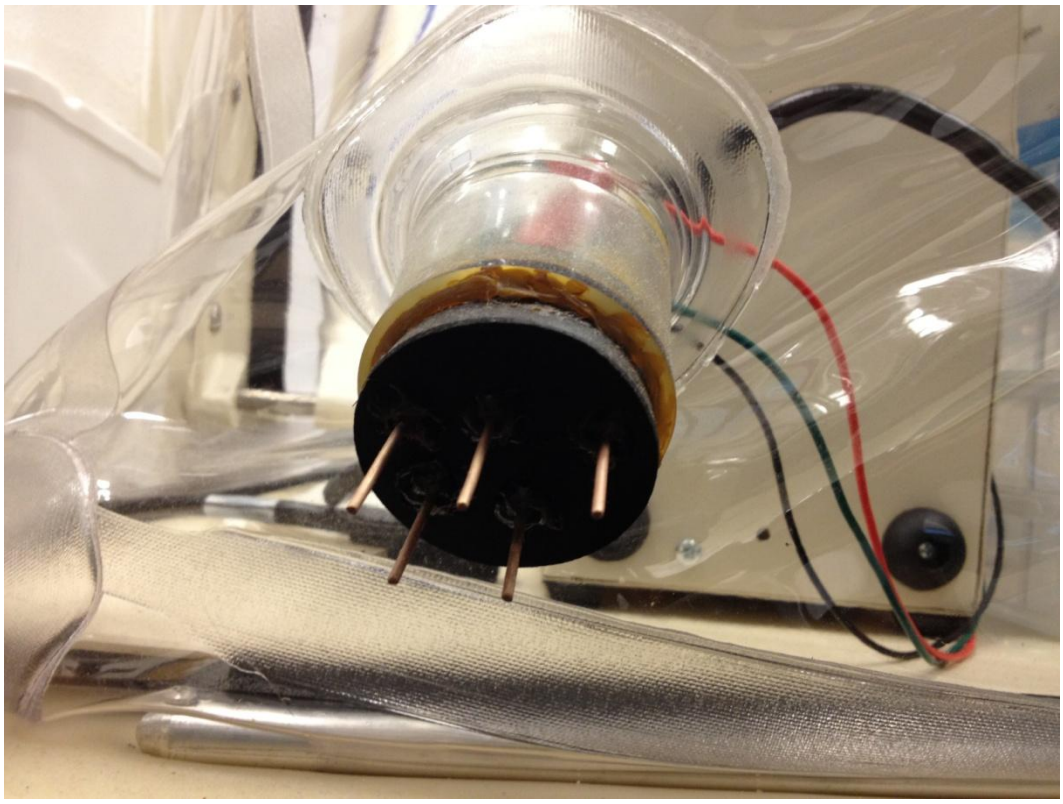

FIGURE 19. Photo of a rubber stopper modified for electrical connections through the anaerobic chamber. The pins are brass and the leads on the inside of the chamber are attached with simple alligator clips.

Most of the electrochemical experiments performed in this dissertation were carried out with electrodes that were fabricated in the lab. PGE electrode construction is described in detail in section 2.1.1 and they are very useful for studying proteins as they adsorb readily to the edge plane graphite surface. The Au (III) substrate construction is described in detail in section 5.3 and these are used for STM studies exclusively due to their atomically flat character. In addition to these electrodes, Ag/AgCl reference electrodes were commonly constructed and freshly made for nearly all electrochemical investigations. Their construction is very simple and easy to do in the lab in a few minutes. To prepare a fresh Ag/AgCl reference, start by polishing a silver wire with sandpaper (~600 grit) until it's shiny and silver. Then, immerse the wire in bleach (sodium hypochlorite) for roughly 5 minutes or until the wire loses its luster and turns dark brown to black (this is the chloride layer on the surface of the silver wire). Next, rinse the wire with water to remove excess bleach and dry it off. Finally place the wire into a glass tube sealed with a Vycor frit at one end and filled with saturated potassium chloride solution. Seal the open end with Teflon tape and it's ready to use by making a connection to the reference lead from the potentiostat. The saturated KCl, Ag/AgCl reference can be converted to the NHE scale by adding 0.199 V to the obtained value.

Miniature gold electrodes were also constructed for initial tests with SAMs and voltammetry experiments. To make these electrodes is rather difficult, but worth it if they turn out nice. To start, 50 µM gold wire must be sealed into a glass tube of an inner diameter of a millimeter or two. This was accomplished

with an oxygen/natural gas flame. The wire was placed through the tube and heated with the flame until the glass melted and completely sealed the wire. This step is critical as bubbles form around the wire when the glass is melted too fast and it doesn't have sufficient time to warm up. It's also possible to heat the entire assembly too much and, either melt the gold which will cause a loss of electrical contact, or melt the glass until it drips and destroys the working edge of the electrode. Once sealed properly, it is crucial to anneal the electrode in a lower temperature flame to cool it off slowly. This step is very tricky as the wire and glass cool at different temperatures and cracks in the glass are common which render the electrode useless for electrochemistry. Once sealed and cooled properly, it is necessary to sand down the electrodes to a flat surface with rough sandpaper followed by subsequent polishing with finer sandpaper. When the electrode is polished as much as it will be with sandpaper, diamond based polishing compound should be used. This comes in a variety of sizes down to 1 μm or less. Following polishing with diamond paste, alumina should be used and the electrode polished until a mirror finish is obtained. Prior to each use, the electrode should be polished with alumina and sonicated in water to remove any excess alumina.

5.6 Anaerobic Chamber Design and Maintenance

Since all hydrogenase work must be performed in an anaerobic chamber, there are extra design considerations that must be taken into account to customize the chamber for hydrogenase work. For example, the chamber in ISTB-V was built in the 1950's for work with inorganic compounds and was not suitable for

electrochemistry or protein work until modifications were made. The entire inside of the chamber was sealed with silicone sealant to keep oxygen out and the door latch mechanism had to be replaced with another, more robust latch. The doors themselves were also modified with silicone sheet and rubber sealant to hold a vacuum and pressure as the chamber was not designed to hold much vacuum or work with gases under pressure. The floor was also modified with rubber to keep equipment from moving around and keep liquid from corroding the floor. Additional electrical connections and pass throughs were installed in one wall of the chamber for electrochemical experiments as well as a quartz window for photoelectrochemical experiments. All of the pass throughs were sealed with silicone and worked well for the duration of a graduate study (5 years) and will likely function for several years to come.

Routine maintenance is absolutely necessary for this glovebox as it is quite old and somewhat unreliable. Regeneration of the palladium catalyst must take place every week or two depending on how much use the chamber sees. The door seals should be checked regularly as this is the most common point of leakage and the only mechanical seal for the chamber. The door latches must also be replaced one a year or so to ensure proper sealing as the rubber wears out quickly. New latches can be ordered from McMaster Carr and a supply of extras can be found in the lab. It's also necessary to open the anaerobic chamber once a year or more to check the silicone sealant on the inside of the chamber and the windows and any other spot that has the potential to leak. The pass throughs for electrical connections are also common spots for leakage and they should be

removed and checked occasionally. The gloves and seals for them should also be checked whenever the chamber is opened as the gloves are another common spot for leakage. The gloves are held into place with a spring clamp, which must be sealed with a light coating of vacuum grease before being replaced to prevent leakage. When closing up the chamber and sealing the windows, it's imperative that the window seals be coated with vacuum grease and the screws be tightened from the center out in a criss-cross pattern to prevent the glass from breaking. Following these tips, the anaerobic chamber will remain operational indefinitely and work with hydrogenase can progress.

5.7 Conclusions

Due to the unique set of experiments that were performed for this dissertation, much of the equipment had to be specifically fabricated to meet the demands of the individual experiment. Other experiments required that existing lab equipment be modified before use. This chapter is intended to inform the reader or investigator of some of the design considerations for these types of experiments. Nearly all of the electrodes used for electrochemical investigations or STM studies were fabricated in the laboratory to meet the needs of the project. The anaerobic chambers that were used for hydrogenase studies were constantly modified and maintained to keep them suitable for continuous use. Design and modification of lab equipment is a work in progress that is constantly evolving to meet the demands of the particular project and with a little ingenuity, any problem can be solved.

CHAPTER 6

CONCLUSIONS AND PERSPECTIVE

While the system described for measuring the turnover of the [FeFe]-hydrogenase *Ca*HydA is a step in the right direction and a great step forward in actually visualizing the surface coverage of protein, there is still room for improvement. Relating the actual surface coverage from STM images to the electrochemical signal allowed for a calculation of enzymatic turnover based on STM images and cyclic voltammetry studies. This dissertation has provided a discussion on some of the latest advancements for measuring the turnover of hydrogenases as well as a system that mimics nonphotochemical quenching and a molecule that acts as an ambipolar transistor. The method for imaging proteins on modified gold electrodes demonstrates the feasibility of such a system to measure the turnover of other redox enzymes; however limitations in the experimental setup and enzyme itself limit current measurements. It has been shown that the catalytic hydrogen production current decreases exponentially with distance from the electrode surface, although no limiting current was observed. Better protein attachment chemistries are needed to eliminate the limitations with the system and measure the maximum turnover of *Ca*HydA.

A fully synthetic system capable of mimicking nonphotochemical quenching has been designed and investigated using a variety of techniques. Under normal (i.e. neutral) conditions, the model shows a reversible electrochemical signal. It was shown that upon the acidification of the solution, an irreversible reduction appeared in the cathodic region. Under these conditions, the

fluorescence from the porphyrin moieties was quenched, releasing the excess energy as heat, analogous to the natural system. The molecular hexad shows that incorporation of self-regulation in response to external stimuli is possible in human-engineered nanosystems for solar energy conversion.

A single molecule ambipolar field effect transistor has been investigated and its properties described. Two molecules were studied, a 1,7-dipyrrolidine-substituted 3,4,9,10-Perylenetetracarboxylic diimide (PTCDI) and an unsubstituted PTCDI with the former displaying ambipolar FET behavior and the latter used as a control displaying only n-type conduction. By substituting the PTCDI block at the 1 and 7 positions, a decrease in the HOMO-LUMO energy gap can be observed, which results in ambipolar behavior. The molecules were studied with spectroscopic methods as well as electrochemical techniques. STM break junction methods were used to measure the conduction mechanisms of the molecules and decipher the ambipolar behavior of the pyrrolidine-substituted molecule.

This dissertation has outlined a variety of projects ranging from protein studies to single molecule measurements, with the common theme being electrochemistry. Electrochemical techniques have proven to be quite powerful in recent years and progress in the understanding of the most fundamental properties of everything from biomolecules to fully synthetic natural mimics. Future work will likely focus on the development of attachment chemistries for proteins and increasing the sensitivity and speed of single molecule techniques. The combination of existing techniques to study new properties of molecules and

biomolecules alike will also be of interest to researchers. This thesis has described some of the latest advancements to these fields and outlined the future directions of research to continue to progress.

REFERENCES

(1) Schiermeier, Q.; Tollefson, J.; Scully, T.; Witze, A.; Morton, O. *Nature* **2008**, *454*, 816-823.

(2) Fihri, A.; Artero, V.; Pereira, A.; Fontecave, M. *Dalton Trans.* **2008**, 5567-5569.

(3) Fihri, A.; Artero, V.; Razavet, M.; Baffert, C.; Leibl, W.; Fontecave, M. *Angew. Chem. Int. Ed.* **2008**, *47*, 564-567.

(4) Wiberg, N. *Inorganic Chemistry*; Academic Press: London, 2001.

(5) Winter, M.; Brodd, R. J. *Chem. Rev.* **2004**, *104*, 4245-4270.

(6) Turner, J. A. *Science* **2004**, *305*, 972-974.

(7) Esswein, A. J.; Nocera, D. G. *Chem. Rev.* **2007**, *107*, 4022-4047.

(8) Reece, S. Y.; Hamel, J. A.; Sung, K.; Jarvi, T. D.; Esswein, A. J.; Pijpers, J. J. H.; Nocera, D. G. *Science*.

(9) Kanan, M. W.; Nocera, D. G. *Science* **2008**, *321*, 1072-1075.

(10) Youngblood, W. J.; Lee, S.-H. A.; Maeda, K.; Mallouk, T. E. *Acc. Chem. Res.* **2009**, *42*, 1966-1973.

(11) Jiao, F.; Frei, H. *Energy Environ.l Sci.* **2010**, *3*, 1018-1027.

(12) Sánchez-Sánchez, C. M.; Montiel, V.; Tryk, D. A.; Aldaz, A.; Fujishima, A. *Pure. Appl. Chem.* **2001**, *73*, 1917-1927.

(13) Gattrell, M.; Gupta, N.; Co, A. *J. Electroanal. Chem* **2006**, *594*, 1-19.

(14) Lindsay, S. M. *Introduction to Nanoscience*; Oxford University Press, USA, 2009.

(15) Bard, A. J.; Faulkner, L. R. *Electrochemical methods: fundamentals and applications*; 2nd ed.; John Wiley and Sons, Inc., 2001.

(16) Güell, A. G.; Díez-Pérez, I.; Gorostiza, P.; Sanz, F. *Anal. Chem.* **2004**, *76*, 5218-5222.

(17) Evans, D. J.; Pickett, C. J. *Chem. Soc. Rev.* **2003**, *32*, 268-275.

(18) Armstrong, F. A. *Curr. Opin. Chem. Biol.* **2004**, *8*, 133-140.

(19) Volbeda, A.; Fontecilla-Camps, J. C. *Coord. Chem. Rev.* **2005**, *249*, 1609-1619.

(20) Vincent, K. A.; Parkin, A.; Armstrong, F. A. *Chem. Rev.* **2007**, *107*, 4366-4413.

(21) Frey, M. *Chem. Bio. Chem.* **2002**, *3*, 153-160.

(22) Vincent, K. A.; Parkin, A.; Lenz, O.; Albracht, S. P. J.; Fontecilla-Camps, J. C.; Cammack, R.; Friedrich, B.; Armstrong, F. A. *J. Am. Chem. Soc.* **2005**, *127*, 18179-18189.

(23) Parkin, A.; Cavazza, C.; Fontecilla-Camps, J. C.; Armstrong, F. A. *J. Am. Chem. Soc.* **2006**, *128*, 16808-16815.

(24) Butt, J. N.; Filipiak, M.; Hagen, W. R. *Eur. J. Biochem* **1997**, *245*, 116-122.

(25) Goldet, G.; Brandmayr, C.; Stripp, S. T.; Happe, T.; Cavazza, C.; Fontecilla-Camps, J. C.; Armstrong, F. A. *J. Am. Chem. Soc.* **2009**, *131*, 14979-14989.

(26) Hambourger, M.; Gervaldo, M.; Svedruzic, D.; King, P. W.; Gust, D.; Ghirardi, M.; Moore, A. L.; Moore, T. A. *J. Am. Chem. Soc.* **2008**, *130*, 2015-2022.

(27) Jones, A. K.; Sillery, E.; Albracht, S. P. J.; Armstrong, F. A. *Chem. Commun.* **2002**, 866-867.

(28) Alonso-Lomillo, M. A.; Rüdiger, O.; Maroto-Valiente, A.; Velez, M.; Rodríguez-Ramos, I.; Muñoz, F. J.; Fernández, V. M.; De Lacey, A. L. *Nano Lett.* **2007**, *7*, 1603-1608.

(29) Guiral-Brugna, M.; Giudici-Orticoni, M. T.; Bruschi, M.; Bianco, P. *J. Electroanal. Chem.* **2001**, *510*, 136-143.

(30) Lamle, S. E.; Vincent, K. A.; Halliwell, L. M.; Albracht, S. P. J.; Armstrong, F. A. *Dalton Trans.* **2003**, 4152-4157.

(31) Johnston, W.; Cooney, M. J.; Liaw, B. Y.; Sapra, R.; Adams, M. W. W. *Enzyme Microb. Technol.* **2005**, *36*, 540-549.

(32) Svedružić, D.; Blackburn, J. L.; Tenent, R. C.; Rocha, J.-D. R.; Vinzant, T. B.; Heben, M. J.; King, P. W. *J. Am. Chem. Soc.* **2011**, *133*, 4299-4306.

(33) Krassen, H.; Stripp, S.; von Abendroth, G.; Ataka, K.; Happe, T.; Heberle, J. *Journal of Biotechnology* **2009**, *142*, 3-9.

(34) Hoeben, F. J. M.; Meijer, F. S.; Dekker, C.; Albracht, S. P. J.; Heering, H. A.; Lemay, S. J. *ACS Nano* **2008**, *2*, 2497-2504.

(35) Léger, C.; Bertrand, P. *Chem. Rev.* **2008**, *108*, 2379-2438.

(36) Rüdiger, O.; Abad, J. M.; Hatchikian, E. C.; Fernandez, V. M.; De Lacey, A. L. *J. Am. Chem. Soc.* **2005**, *127*, 16008-16009.

(37) Rüdiger, O.; Gutiérrez-Sánchez, C.; Olea, D.; Periera, I. A. C.; Vélez, M.; Fernández, V. M.; De Lacey, A. L. *Electroanalysis* **2010**, *22*, 776-783.

(38) Léger, C.; Jones, A. K.; Albracht, S. P. J.; Armstrong, F. A. *J. Phys. Chem. B.* **2002**, *106*, 13058-13063.

(39) Armstrong, F. A. *J. Chem Soc., Dalton Trans.* **2002**, 661-671.

(40) Heering, H. A.; Hirst, J.; Armstrong, F. A. *J. Phys. Chem. B* **1998**, *102*, 6889-6902.

(41) Pershad, H. R.; Duff, J. L. C.; Heering, H. A.; Duin, E. C.; Albracht, S. P. J.; Armstrong, F. A. *Biochemistry* **1999**, *38*, 8992-8999.

(42) Nakamura, C.; Mizutani, W.; Lantz, M. A.; Noda, K.; Zorin, N. A.; Miyake, J. *Supramolecular Science* **1998**, *5*, 639-642.

(43) Song, S.; Clark, R. A.; Bowden, E. F.; Tarlov, M. J. *J. Phys. Chem.* **1993**, *97*, 6564-6572.

(44) Haas, A. S.; Pilloud, D. L.; Reddy, K. S.; Babcock, G. T.; Moser, C. C.; Blasie, J. K.; Dutton, P. L. *J. Phys. Chem. B* **2001**, *105*, 11351-11362.

(45) Léger, C.; Dementin, S.; Bertrand, P.; Rousset, M.; Guigliarelli, B. *J. Am. Chem. Soc.* **2004**, *126*, 12162-12172.

(46) Léger, C.; Jones, A. K.; Roseboom, W.; Albracht, S. P. J.; Armstrong, F. A. *Biochemistry* **2002**, *41*, 15736-15746.

(47) King, P. W.; Posewitz, M. C.; Ghirardi, M. L.; Seibert, M. *J. Bacteriol.* **2006**, *188*, 2163-2172.

(48) Peters, J. W.; Lanzilotta, W. N.; Lemon, B. J.; Seefeldt, L. C. *Science* **1998**, *282*, 1853-1858.

(49) Pandy, A. S.; Harris, T. V.; Giles, L. J.; Peters, J. W.; Szilagyi, R. K. *J. Am. Chem. Soc.* **2008**, *130*, 4533-4540

(50) Adams, M. W. W.; Mortenson, L. E. *J. Biol. Chem.* **1984**, *259*, 7045-7055.

(51) Baffert, C.; Demuez, M.; Cournac, L.; Burlat, B.; Guigliarelli, B.; Bertrand, P.; Girbal, L.; Léger, C. *Angew. Chem. Int. Ed.* **2008**, *47*, 2052-2054.

(52) Adams, M. W. W. *Biochim. Biophys. Acta* **1990**, *1020*, 115-145.

(53) Stookey, L. L. *Anal. Chem.* **1971**, *42*, 779-781.

(54) Carter, P. *Anal. Biochem.* **1970**, *40*, 450-458.

(55) Schägger, H. *Nature Protocols* **2006**, *1*, 16-22

(56) Schägger, H.; von Jagow, G. *Anal. Biochem.* **1987**, *166*, 368-379.

(57) Winkler, C.; Denker, K.; Wortelkamp, S.; Sickmann, A. *Electrophoresis* **2007**, *28*, 2095-2099.

(58) Sali, A.; Blundell, T. L. *Journal of Molecular Biology* **1993**, *234*, 779-815.

(59) Im, W.; Beglov, D.; Roux, B. *Computer Physics Communications* **1998**, *111*, 59-75

(60) Jo, S.; Vargyas, M.; Vasco-Szedlar, J.; Roux, B.; Im, W. *Nucleic Acids Research* **2008**, *36*, W270-W275.

(61) Humphrey, W.; Schulten, K.; Dalke, A. *Journal of molecular graphics* **1996**, *14*, 33-38.

(62) Kubiak-Ossowska, K.; Mulheran, P. A. *Langmuir* **2010**, *26*, 7690-7694.

(63) Brown, K. A.; Dayal, S.; Ai, X.; Rumbles, G.; King, P. W. *J. Am. Chem. Soc.* **2010**, *132*, 9672-9680

(64) Bianco, P.; Haladjian, J. *J. Electrochem. Soc.* **1992**, *139*, 2428-2432.

(65) Chi, Q.; Farver, O.; Ulstrup, J. *Proc. Nat. Acad. Sci. U.S.A.* **2005**, *102*, 16203-16208.

(66) Tao, N. J. *Phys. Rev. Lett.* **1996**, *76*, 4066-4069.

(67) Cui, X. D.; Zarate, X.; Tomfohr, J.; Sankey, O. F.; Primak, A.; Moore, A. L.; Moore, T. A.; Gust, D.; Harris, G.; Lindsay, S. M. *Nanotechnology* **2002**, *13*, 5-14.

(68) Allongue, P.; Delamar, M.; Desbat, B.; Fagebaum, O.; Hitmi, R.; Pinson, J.; Savéant, J.-M. *J. Am. Chem. Soc.* **2007**, *119*, 201-207.

(69) Blankenship, R. E. *Molecular mechanisms of photosynthesis*; Blackwell Science, Ltd.: Malden, MA, 2002.

(70) Sørenson, B. *Renewable Energy: Its Physics, Engineering, Environmental Impacts, Economics & Planning*; 4th ed.; Elsevier Academic Press: Burlington, MA 2010.

(71) Lewis, N. S.; Nocera, D. G. *Proc. Nat. Acad. Sci., USA* **2006**, *103*, 15729-15735.

(72) Reece, S. Y.; Hamel, J. A.; Sung, K.; Jarvi, T. D.; Esswein, A. J.; Pijpers, J. J. H.; Nocera, D. G. *Science* **2011**, *334*, 645-648.

(73) Gust, D.; Moore, T. A.; Moore, A. L. *Acc. Chem. Res.* **2001**, *34*, 40-48.

(74) Gust, D.; Moore, T. A.; Moore, A. L. *Acc.Chem. Res.* **2009**, *42*, 1890-1898.

(75) Demmig-Adams, B.; Adams, W. W. *Science* **2002**, *298*, 2149-2153.

(76) Ruban, A. V.; Berera, R.; Ilioaia, C.; van Stokkum, I. H. M.; Kennis, J. T. M.; Pascal, A. A.; van Amerongen, H.; Robert, B.; Horton, P.; van Grondelle, R. *Nature* **2007**, *450*, 575-578.

(77) Kyu Ahn, T.; Avenson, T. J.; Ballottari, M.; Cheng, Y.-C.; Niyogi, K. K.; Bassi, R.; Fleming, G. R. *Science* **2008**, *320*, 794-797.

(78) Terazono, Y.; Kodis, G.; Bhushan, K.; Zaks, J.; Madden, C.; Moore, A. L.; Moore, T. A.; Fleming, G. R.; Gust, D. *J. Am. Chem. Soc.* **2011**, *133*, 2916-2922.

(79) Barzilay, C. M.; Sibilia, S. A.; Spiro, T. G.; Gross, Z. *Chemistry – A European Journal* **1995**, *1*, 222-231.

(80) Aviram, A.; Ratner, M. A. *Chem. Phys. Lett.* **1974**, *29*, 277-283.

(81) Xu, B.; Tao, N. J. *Science* **2003**, *301*, 1221-1223.

(82) Díez-Pérez, I.; Hihath, J.; Lee, Y.; Yu, L.; Adamska, L.; Kozhushner, M. A.; Oleynik, I. I.; Tao, N. *Nat. Chem.* **2009**, *1*, 635-641.

(83) Diez-Perez, I.; Li, Z.; Hihath, J.; Li, J.; Zhang, C.; Yang, X.; Zang, L.; Dai, Y.; Feng, X.; Muellen, K.; Tao, N. *Nat. Commun.*, *1*, 31.

(84) Artés, J. M.; Díez-Pérez, I.; Gorostiza, P. *Nano Lett*. dx.doi.org/10.1021/nl2028969

(85) Matsumura, M.; Nara, Y. *J. Appl. Phys.* **1980**, *51*, 6443-6344.

(86) Heinze, S.; Radosavljević, M.; Tersoff, J.; Avouris, P. *Physical Review B* **2003**, *68*, 235418.

(87) Novoselov, K. S.; Geim, A. K.; Morozov, S. V.; Jiang, D.; Zhang, Y.; Dubonos, S. V.; Grigorieva, I. V.; Firsov, A. A. *Science* **2004**, *306*, 666-669.

(88) Dodabalapur, A.; Katz, H. E.; Torsi, L.; Haddon, R. C. *Science* **1995**, *269*, 1560-1562.

(89) Yuen, J. D.; Fan, J.; Seifter, J.; Lim, B.; Hufschmid, R.; Heeger, A. J.; Wudl, F. *J. Am. Chem. Soc.*, *133*, 20799-20807.

(90) Yuan, H.; Liu, H.; Shimotani, H.; Guo, H.; Chen, M.; Xue, Q.; Iwasa, Y. *Nano Lett.*, *11*, 2601-2605.

(91) Chikamatsu, M.; Mikami, T.; Chisaka, J.; Yoshida, Y.; Azumi, R.; Yase, K.; Shimizu, A.; Kubo, T.; Morita, Y.; Nakasuji, K. *Appl. Phys. Lett.* **2007**, *91*.

(92) Ye, J. T.; Inoue, S.; Kobayashi, K.; Kasahara, Y.; Yuan, H. T.; Shimotani, H.; Iwasa, Y. *Nat. Mater.*, *9*, 125-128.

(93) Martineau, D.; Beley, M.; Gros, P. C. *J. Org. Chem.* **2005**, *71*, 566-571.

(94) Haiss, W.; Nichols, R. J.; van Zalinge, H.; Higgins, S. J.; Bethell, D.; Schiffrin, D. J. *Physi. Chem. Chem. Phys.* **2004**, *6*.

(95) Chang, S.; He, J.; Kibel, A.; Lee, M.; Sankey, O.; Zhang, P.; Lindsay, S. *Nat. Nano.* **2009**, *4*, 297-301.

(96) Xu, B.; Xiao, X.; Yang, X.; Zang, L.; Tao *J. Am. Chem. Soc.* **2005**, *127*, 2386-2387.

(97) Li, X.; Hihath, J.; Chen, F.; Masuda, T.; Zang, L.; Tao *J. Am. Chem. Soc.* **2007**, *129*, 11535-11542.

(98) Zhang, J.; Kuznetsov, A. M.; Ulstrup, J. *J. Electroanal. Chem.* **2003**, *541*, 133-146.